J. Fluid Mech. (2006), *vol.* 551, *pp.* 275–301.
doi:10.1017/S0022112005008323 Printed in the United Kingdom

Three-dimensional global instability modes associated with a localized hot spot in Rayleigh–Bénard–Poiseuille convection

By DENIS MARTINAND[1,2]†, PHILIPPE CARRIÈRE[1] AND PETER A. MONKEWITZ[2]

[1]Laboratoire de Mécanique des Fluides et d'Acoustique, UMR CNRS 5509, Ecole Centrale de Lyon – Université Claude Bernard Lyon I – INSA Lyon, 69134 Ecully cedex, France

[2]Laboratoire de Mécanique des Fluides, Ecole Polytechnique Fédérale de Lausanne, CH-1015, Lausanne, Switzerland

(Received 8 November 2004 and in revised form 8 September 2005)

Global modes of the thermal convection type in the Rayleigh–Bénard–Poiseuille (RBP) system are analysed for the case of non-uniform heating of the lower wall. Specifically, a single two-dimensional 'hot spot' or 'temperature bump' giving rise to a finite region of local instability is considered. For the case of the lower wall temperature varying slowly on the scale of the RBP cell height, i.e. for a gentle temperature bump, WKBJ asymptotics are used to construct an analytical approximation of the linear global mode. At the same time, an analytical selection criterion for the critical global mode is derived from the breakdown of the WKBJ expansion at a double turning point located at the top of the temperature bump. The analytical construction and the underlying assumptions are supported by comparison with direct numerical simulations for Gaussian temperature bumps of elliptical planform not necessarily aligned with the mean flow. From these comparisons, it is concluded that the proposed analytical construction indeed yields the most amplified global mode, which is characterized by an essentially transverse orientation (normal to the mean flow direction) of the convection rolls, independent of the planform of the temperature bump. The paper concludes with preliminary DNS results on the saturated global mode shape and a discussion of possible connections to the 'steep' fully nonlinear global modes found for one-dimensional inhomogeneities of the basic state.

1. Introduction

Most instabilities of practical interest are developing on 'imperfect' basic states, i.e. on basic states which are spatially inhomogeneous or spatially varying in more than one direction. For certain inhomogeneities, such systems can develop instabilities which remain spatially localized. Among those, we will focus on localized instabilities which are temporally synchronized (which have the same frequency and temporal linear growth rate throughout the field). Such instabilities are referred to as 'global modes'. Once destabilized, they are self-excited and represent an intrinsic response of the basic state to an infinitesimal, but

† Present address: Laboratoire de Physique, ENS Lyon, 46 allée d'Italie, F-69007 Lyon, France.

otherwise arbitrary initial disturbance, i.e. the same global mode results from any sufficiently small initial disturbance. In this sense, an unstable global mode in an inhomogeneous system is perfectly analogous to an absolute instability in a parallel or homogeneous system (see Huerre & Monkewitz 1990). The classic example for global modes is the von Kármán vortex street in two-dimensional bluff-body wakes (see e.g. Provansal, Mathis & Boyer 1987; Roussopoulos & Monkewitz 1996).

The above mentioned characteristics of a self-tuned instability or global mode imply that the corresponding linear stability analysis has to provide a selection criterion which predicts the intrinsic global mode frequency, temporal growth rate and mode shape for a given set of control parameters. This selection criterion is a consequence of both the inhomogeneity of the basic state and the physical instability mechanism(s). Since the latter vary spatially in strength or even in nature within an inhomogeneous system, the frequency selection criterion for a global mode cannot be simply derived from an algebraic dispersion relation. This situation is unlike that encountered in parallel systems, where the standard linear stability analysis results in the dispersion relation in which all but one parameter can be chosen freely.

Whereas an arbitrary variation of the basic state is usually accessible to stability analysis only through experiments or numerical simulations, a 'slow' variation of the basic state (relative to a characteristic instability length scale) opens the door to analytical investigations. The slow variation justifies a first approximation consisting of treating the system as locally parallel, and hence, the location appears only as a parameter in the local homogeneous stability problems. This is analogous to optics where light propagation through inhomogeneous media can be described by the eikonal equation of geometrical optics when the wavelength is small compared to the scale of the inhomogeneities. For historical reasons, such an approximation is called the WKBJ expansion after Wentzel–Kramers–Brillouin–Jeffreys (see Jammer 1966; Bender & Orszag 1978, for mathematical and historical developments). Since the leading WKBJ approximation for the linear global modes to be considered here is given by the solutions of the local homogeneous (linear) stability problem, it is intuitively clear that the concept of (local) absolute instability, defined by the linear impulse response and introduced in hydrodynamics by Huerre & Monkewitz (1985), plays an important role in the analysis of global modes in weakly non-parallel systems. Physically speaking, local absolute instability is associated with zero group velocity of the local absolute instability modes and hence permits perturbation energy to 'accumulate in place'. From the above, it is clear that a global mode selection criterion cannot be obtained from the leading order (geometrical optics) WKBJ approximation. We therefore have to proceed to the next order (to physical optics) which determines how the different local solutions inter-relate. In the WKBJ formalism, this is described by a slowly varying amplitude which multiplies the leading-order approximation. This physical optics approximation can, however, break down, as the governing equation for the slowly varying amplitude can have turning points where the coefficients of the highest derivative(s) vanish. For systems presenting a one-dimensional slowly varying basic state, such turning points have been related to selection criteria and the intrinsic behaviour of the instability, first for arbitrary dynamic equations (Huerre & Monkewitz 1990; Chomaz, Huerre & Redekopp 1991; Le Dizès *et al.* 1996), then for more realistic flows as, for instance, spatially developing shear flows (Monkewitz, Huerre & Chomaz 1993) and more recently Rayleigh–Bénard–Poiseuille (RBP) convection (Carrière & Monkewitz 2001).

It appears that this last system, in which a low-Reynolds-number laminar Poiseuille flow is added to the Rayleigh–Bénard (RB) thermal convection cell, is a valuable 'guinea-pig' to study global instabilities, as it exhibits a transition between convective and absolute instability (see Carrière & Monkewitz 1999) and is closely related to the extensively documented RB system. In addition, particular inhomogeneities of the system, such as lateral confinement or a thermal entry, have already been studied experimentally and numerically and are known to influence strongly the morphology of the instability (see Kelly 1994; Nicolas 2002, for a review). Finally, an inhomogeneity in the RBP system can be realized in a natural fashion by spatially variable heating of the bottom wall, for instance, thereby creating a 'temperature bump' in the boundary condition.

The present study extends the analytical procedure presented in Martinand, Carrière & Monkewitz (2004, hereinafter referred to as MCM04), where an envelope formalism was used to analyse synchronized global modes in RBP systems which are inhomogeneous in all three space directions ('slow' inhomogeneity in the two horizontal directions and the usual 'fast' inhomogeneity in the vertical direction). The validity of the envelope equation, derived from the Navier–Stokes equations with the Boussinesq approximation, was, however, limited *a priori* to transverse rolls (with axes perpendicular to the mean flow direction) and to near-critical conditions with infinitesimal Reynolds number, as discussed in Carrière, Monkewitz & Martinand (2004). Furthermore, owing to the different scalings of the streamwise and transverse directions in the envelope equation, the temperature bumps had to be restricted to mirror-symmetric shapes with respect to at least one horizontal coordinate axis. These restrictions imposed on the envelope formalism effectively prevent its use as a model even for a practical laboratory experiment, not to speak of any system of more technological interest. To relax them, the WKBJ global mode analysis has to be carried out on the governing equations (continuity, Navier–Stokes and energy equations with the Boussinesq approximation) themselves rather than on the envelope equation as in MCM04. The present study also builds on previous analysis handling the full set of equations, but restricted to a single slowly varying direction in RBP convection (Carrière & Monkewitz 2001).

This is the general programme for the present study. Specifically, we analyse the situation where the cold top wall is held at a constant temperature and the bottom wall temperature has a slowly varying two-dimensional bump, such that the region of local instability is compact, i.e. such that the system is stable away from the finite-sized temperature bump. In the following, we focus on global modes for this type of inhomogeneity. These modes will appear to comply with the mechanisms of selection and the principles of construction determined for one-dimensional bumps in Carrière & Monkewitz (2001). Consequently, the analytical part of this paper concentrates on technical issues raised by the two slowly varying directions. A thorough account of this analysis can be found in Martinand (2003).

The paper is organized as follows. In § 2, the slowly varying basic state, which can no longer be expressed analytically because of the temperature bump, is determined in the form of a power series in the small parameter ε, defined as the ratio of the instability wavelength (or roll diameter) to the characteristic dimension of the bump, i.e. characterizing the slowness of the spatial variation in the horizontal directions. In § 3, the instability on this inhomogeneous basic state is expressed as the leading order of a WKBJ expansion in terms of ε, and the breakdown of this WKBJ expansion at turning points is discussed. At this point, the choice is made to consider global modes associated with a double turning point in both horizontal space directions and

this turning-point region is analysed in § 4. From the matching requirements between this 'inner' turning-point solution and the 'outer' WKBJ solution, the sought-after global mode selection criterion is finally expressed. Then, the choice of the double turning point for the construction of the global mode and different assumptions of a more technical nature are then justified in § 5 by comparison with direct numerical simulations. In the final § 6, the usefulness of the developed analytical global mode approximation is demonstrated with a parametric study looking into the effect of Prandtl number and of the maximum lower wall temperature (the bump height) on the global instability threshold, and some DNS results on the nonlinear stages of the global mode evolution are presented.

2. Basic state

We consider a flow imposed by a horizontal pressure gradient and bounded by two differentially heated horizontal walls, where the upper wall is held at the constant temperature $\Theta_u^\dagger$ (throughout the paper, the † identifies dimensional quantities but has been omitted for univocal parameters and coefficients which are *de facto* dimensional), while the temperature of the lower wall $\Theta_l^\dagger(x^\dagger, y^\dagger)$ is a function of both horizontal coordinates $x^\dagger$ and $y^\dagger$. In the following, it is assumed that the function $\Theta_l^\dagger(x^\dagger, y^\dagger)$ has a single maximum $\Theta_{l,0}^\dagger$ at $x^\dagger = y^\dagger = 0$ and tends to a constant lower bound $\Theta_{l,\infty}^\dagger$ as $x^\dagger \to \pm\infty$ or $y^\dagger \to \pm\infty$. Typically, $\Theta_{l,\infty}^\dagger$ will be chosen such that the RBP system is locally stable far away from the temperature 'bump' at the origin. Furthermore, we focus on situations where the lower wall temperature $\Theta_l^\dagger(x^\dagger, y^\dagger)$ varies slowly on the scale of the gap between the horizontal walls. This is expressed by making $\Theta_l^\dagger$ dependent on slow variables $X^\dagger$ and $Y^\dagger$ alone, where slow and rapid variables are linked by $X^\dagger = \varepsilon x^\dagger$ and $Y^\dagger = \varepsilon y^\dagger$, with $\varepsilon \ll 1$ a small parameter characterizing the deviation from spatially homogeneous conditions.

The velocity, pressure and temperature fields – $\boldsymbol{U}^\dagger$, $P^\dagger$ and $\Theta^\dagger$, respectively – are solutions of the continuity, Navier–Stokes and energy equations simplified by the Boussinesq approximation, i.e. with constant density except in the buoyancy term and constant transport coefficients:

$$\boldsymbol{\nabla}\cdot\boldsymbol{U}^\dagger = 0, \tag{2.1a}$$

$$\partial_{t^\dagger}\boldsymbol{U}^\dagger + (\boldsymbol{U}^\dagger\cdot\boldsymbol{\nabla})\boldsymbol{U}^\dagger + \frac{1}{\rho}\boldsymbol{\nabla}P^\dagger - \alpha(\Theta^\dagger - \Theta_r^\dagger)g\boldsymbol{e}_z - \nu\boldsymbol{\nabla}^2\boldsymbol{U}^\dagger = \boldsymbol{0}, \tag{2.1b}$$

$$\partial_{t^\dagger}\Theta^\dagger + (\boldsymbol{U}^\dagger\cdot\boldsymbol{\nabla})\Theta^\dagger - \kappa\boldsymbol{\nabla}^2\Theta^\dagger = 0, \tag{2.1c}$$

with the following boundary conditions:

$$\boldsymbol{U}^\dagger(z^\dagger = \pm h/2) = \boldsymbol{0}, \tag{2.2a}$$

$$\Theta^\dagger(z^\dagger = h/2) = \Theta_u^\dagger, \tag{2.2b}$$

$$\Theta^\dagger(z^\dagger = -h/2) = \Theta_l^\dagger(X^\dagger, Y^\dagger), \tag{2.2c}$$

where the coordinate origin is taken to be halfway between the horizontal walls spaced apart by h, ρ the density, g the acceleration due to gravitational in the negative z-direction, ν the kinematic viscosity, α the thermal expansion coefficient and κ the thermal diffusivity (all these parameters being dimensional) at the reference temperature $\Theta_r^\dagger = \Theta_u^\dagger$.

The basic state, on which the global mode analysis will be performed, is the steady laminar solution $\boldsymbol{U}^\dagger = (U^\dagger, V^\dagger, W^\dagger)$ of system (2.1) which is sought in terms of a

power series in ε. Taking the leading-order pressure gradient to be aligned with the x-direction, it reads

$$P_b^\dagger(x^\dagger, X^\dagger, Y^\dagger, z^\dagger) = \frac{\rho\nu\kappa}{h^2}\{P_0(x, X, Y, z) + \varepsilon P_1(X, Y, z) + O(\varepsilon^2)\}, \tag{2.3a}$$

$$\boldsymbol{U}_b^\dagger(X^\dagger, Y^\dagger, z^\dagger) = \boldsymbol{U}_m^\dagger \boldsymbol{U}_0(X, Y, z) + \varepsilon\frac{\kappa}{h}\boldsymbol{U}_1(X, Y, z) + O(\varepsilon^2), \tag{2.3b}$$

$$\Theta_b^\dagger(X^\dagger, Y^\dagger, z^\dagger) - \Theta_u^\dagger = \frac{\nu\kappa}{\alpha g h^3}\{\Theta_0(X, Y, z) + \varepsilon\Theta_1(X, Y, z) + O(\varepsilon^2)\}, \tag{2.3c}$$

where non-dimensional quantities (without †) have been introduced as follows:

lengths are made non-dimensional with h,

velocities with the thermal diffusion velocity κ/h, except for the leading-order velocity $\boldsymbol{U}_0^\dagger$ in the expansion (2.3) which is made non-dimensional with the maximum velocity $\boldsymbol{U}_m^\dagger$ of the Poiseuille flow induced by $\partial_x P_b^\dagger$,

time with h^2/κ,

pressure with $\rho\nu\kappa/h^2$ and

temperature with $\nu\kappa/(\alpha g h^3)$.

The resulting non-dimensional control parameters are

Reynolds number $R = U_m^\dagger h/\nu$,

Prandtl number $P = \nu/\kappa$ and

local Rayleigh number $\mathscr{R}(X, Y) = (\alpha g h^3)(\Theta_l^\dagger(X^\dagger, Y^\dagger) - \Theta_u^\dagger)/(\nu\kappa)$, based on the local temperature difference between the upper and lower walls. It has a lower bound $\mathscr{R}_\infty$ far away from the origin where $\Theta_l^\dagger = \Theta_{l,\infty}^\dagger$ and a single maximum $\mathscr{R}_0$ at the origin $(X, Y) = (0, 0)$ where $\Theta_l^\dagger = \Theta_{l,0}^\dagger$.

The orders $O(\varepsilon^0)$ and $O(\varepsilon)$ of the basic state (2.3) are evaluated in a similar fashion to § 2 of Carrière & Monkewitz (2001). It yields at leading order $O(\varepsilon^0)$:

$$P_0 = \widetilde{P_0}(z)\mathscr{R} - 8RPx + \tfrac{1}{40}[\mathscr{R} - \mathscr{R}_\infty];\ \widetilde{P_0}(z) = \tfrac{1}{2}z(1-z), \tag{2.4a}$$

$$U_0 = 1 - 4z^2, \tag{2.4b}$$

$$V_0 = 0, \tag{2.4c}$$

$$W_0 = 0, \tag{2.4d}$$

$$\Theta_0 = \widetilde{\Theta_0}(z)\mathscr{R};\ \widetilde{\Theta_0}(z) = \tfrac{1}{2} - z. \tag{2.4e}$$

As expected, the homogeneous Poiseuille flow aligned with the leading-order pressure gradient in the x-direction and the pure conduction solution for the temperature are recovered.

The order $O(\varepsilon)$ contribution to the basic state, which, compared with Carrière & Monkewitz (2001), also has a velocity component in the spanwise y-direction, is obtained as:

$$P_1 = RP\widetilde{P_1}(z)\partial_X\mathscr{R} + H;\ \widetilde{P_1}(z) = \tfrac{z}{480}(16z^5 - 16z^4 - 20z^3 + 40z^2 + 7z + 25), \tag{2.5a}$$

$$U_1 = -\widetilde{U_1}(z)\partial_X\mathscr{R}, \tag{2.5b}$$

$$V_1 = -\widetilde{U_1}(z)\partial_Y\mathscr{R};\ \widetilde{U_1}(z) = \left(z - \tfrac{1}{2}\right)\left(z + \tfrac{1}{2}\right)\left(\frac{z^2}{24} - \frac{z}{12} - \frac{7}{480}\right), \tag{2.5c}$$

$$W_1 = 0, \tag{2.5d}$$

$$\Theta_1 = -RP\widetilde{\Theta_1}(z)\partial_X\mathscr{R};\ \widetilde{\Theta_1}(z) = \tfrac{1}{120}\left(z - \tfrac{1}{2}\right)\left(z + \tfrac{1}{2}\right)(24z^3 - 20z^2 - 14z + 25), \tag{2.5e}$$

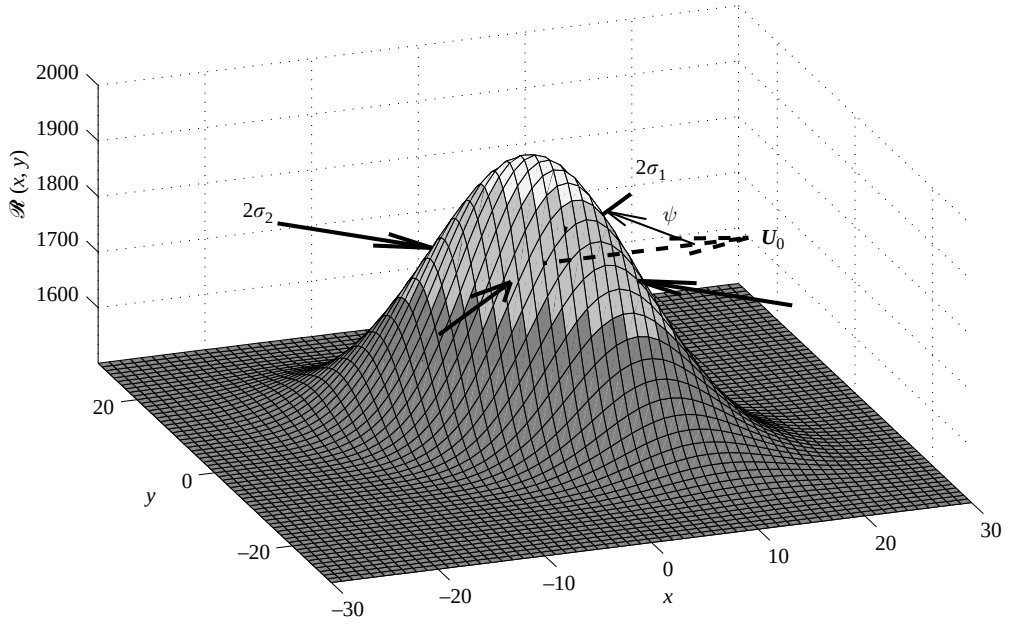

FIGURE 1. Example of the local Rayleigh number $\mathscr{R}$ for a Gaussian temperature bump with $\sigma_1 = 5$, $\sigma_2 = 10$ and $\psi = \pi/4$. The local stability properties, evaluated for $R = 0.85$ and $P = 7$ as in Carrière & Monkewitz (1999), are shown by shading with increasingly lighter shades of grey for the stable, convectively unstable and absolutely unstable regions.

The only remaining unknown function is $H(X, Y)$ in P_1. It can be determined at the next order, $O(\varepsilon^2)$. However, since P_1 will not appear in the following formulation of the stability problem, the determination of $H(X, Y)$ is not necessary. To revert to unstretched coordinates in (2.5) for the first-order corrections, the derivatives ∂_X and ∂_Y are simply replaced by $\varepsilon^{-1}\partial_x$ and $\varepsilon^{-1}\partial_y$.

Expressions (2.4) and (2.5) remain valid for any slow function $\mathscr{R}$ of x and y. To illustrate the approximation of the basic state and to construct examples of global modes in the following sections, a Gaussian temperature bump or 'hot spot' with an elliptic planform is used, from which a local Rayleigh number is deduced:

$$\mathscr{R}(x, y) = \mathscr{R}_\infty + (\mathscr{R}_0 - \mathscr{R}_\infty) \times \exp\left[-\frac{x^2}{2}\left(\frac{\cos^2\psi}{\sigma_1^2} + \frac{\sin^2\psi}{\sigma_2^2}\right) - \frac{y^2}{2}\left(\frac{\sin^2\psi}{\sigma_1^2} + \frac{\cos^2\psi}{\sigma_2^2}\right) - \frac{xy}{2}\sin 2\psi\left(\frac{1}{\sigma_1^2} - \frac{1}{\sigma_2^2}\right)\right], \tag{2.6}$$

where ψ is the angle between the x-axis and the principal axis '1' of the elliptic temperature bump.

An example of such a bump is shown in figure 1, together with the parameters used for its definition, and the corresponding first two orders of the basic state, given by (2.4) and (2.5), are presented in figure 2.

3. WKBJ analysis of linear global modes

This section is devoted to the linear stability analysis of the basic state derived in the previous section. For this, a time-dependent perturbation $\boldsymbol{v} = {}^{\mathrm{T}}(p, u, v, w, \theta)$ (the

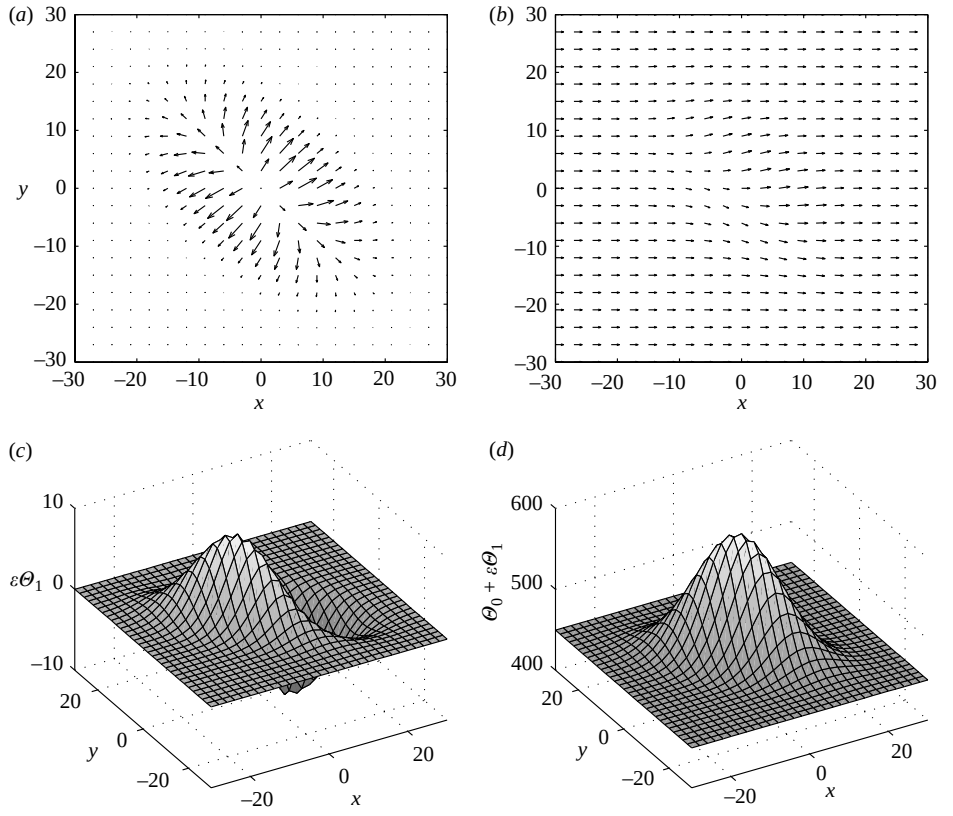

FIGURE 2. Basic state corresponding to $\mathscr{R}$ of figure 1 at $z = 0.2$. (a, c) First-order corrections $\varepsilon \boldsymbol{V}_1$ and $\varepsilon\Theta_1$. (b, d) First two orders $\boldsymbol{V}_0 + \varepsilon \boldsymbol{V}_1$ and $\Theta_0 + \varepsilon\Theta_1$.

$^{\mathrm{T}}$ standing for transpose) is added to the basic steady state $^{\mathrm{T}}(P_b, U_b, V_b, W_b, \Theta_b)$. The instability is sought as a synchronized global mode, for which the complex frequency ω is the same in the whole physical domain, but otherwise unknown. As the dynamics of such an instability are intrinsic, ω must emerge from the global mode construction itself, as shown in the next section.

Owing to the slow spatial variation of the basic state characterized by $\varepsilon \ll 1$, the global mode is constructed as a WKBJ expansion (its domain of validity will be discussed at the end of this section) and the perturbation is expressed using the standard WKBJ ansatz:

$$\boldsymbol{v} = \{\boldsymbol{v}_0(X, Y, z; \omega) + \varepsilon \boldsymbol{v}_1(X, Y, z; \omega) + O(\varepsilon^2)\} \exp\left[\frac{\mathrm{i}}{\varepsilon}\Phi(X, Y) - \mathrm{i}\omega t\right] + \text{c.c.}, \qquad (3.1)$$

with the complex frequency expanded as

$$\omega = \omega_0 + \varepsilon\omega_1 + O(\varepsilon^2) \qquad (3.2)$$

and the wavevector $\boldsymbol{k}$ related to the phase Φ by

$$\boldsymbol{k}(X, Y) = \nabla\Phi(X, Y). \qquad (3.3)$$

Its components are denoted by k_x and k_y and its norm by k. The stability equations at the different orders in ε are deduced from system (2.1), non-dimensionalized as stated in § 2 and linearized about the basic state.

Since obtaining the equations satisified by the leading order of the WKBJ expansion builds on the analytical approaches presented in Carrière & Monkewitz (2001) and MCM04, only a condensed analysis is presented here.

3.1. *Leading order of the WKBJ expansion*

The stability equations at order $O(\varepsilon^0)$ imply that $\boldsymbol{v}_0$ is a solution of the homogeneous local problem pertaining to a fixed station (X, Y). This problem takes the form of the generalized eigenproblem (A 1) in the Appendix with eigenvalue ω_0:

$$\mathscr{M}\boldsymbol{v}_0 - \omega_0 \mathscr{N}\boldsymbol{v}_0 = \boldsymbol{0} \tag{3.4}$$

and vanishing boundary conditions (A 4). In (3.4), operators $\mathscr{M}$ and $\mathscr{N}$ are given by (A 2) and (A 3), respectively. The leading order of the perturbation (3.1) is then sought in the form:

$$\boldsymbol{v}_0 = A(X, Y)\widehat{\boldsymbol{v}_0}(k_x(X, Y), k_y(X, Y), \mathscr{R}(X, Y); \omega_0; z), \tag{3.5}$$

where $\widehat{\boldsymbol{v}_0}$ is conveniently normalized and $A(X, Y)$, the amplitude of the leading order of the WKBJ expansion (3.5), is hereinafter simply referred to as 'the amplitude'.

Since X and Y appear only as parameters, the eigenvalue problem (3.4) with boundary conditions (A 4) yields the local dispersion relation between the wavevector $\boldsymbol{k}$, the leading-order frequency ω_0 and the three control parameters $\mathscr{R}(X, Y)$, R and P:

$$\mathscr{D}(k_x, k_y, \mathscr{R}, \omega_0, R, P) = 0 \tag{3.6}$$

together with the continuity of phase:

$$\partial_Y k_x = \partial_X k_y. \tag{3.7}$$

Restricting the dispersion relation to the most unstable eigenvalue for ω_0 and considering R and P fixed, (3.6) and (3.7) are equivalent to the following first-order nonlinear partial differential equation satisfied by Φ:

$$\omega(\partial_X \Phi, \partial_Y \Phi, \mathscr{R}) = \omega_0. \tag{3.8}$$

Note here that the function ω should not be confused with the global mode frequency (3.2). Since we have assumed that the locally unstable region is confined to the neighbourhood of the origin and we are excluding any forcing of the global modes, their amplitude must vanish far from the origin. Since $\exp(\mathrm{i}\Phi(X, Y)/\varepsilon)$ is dominant for $\varepsilon \to 0$, Φ must satisfy the condition:

$$\mathrm{Im}(\Phi) \to \infty \text{ as } X \to \pm\infty \text{ or } Y \to \pm\infty. \tag{3.9}$$

In a similar fashion to one-dimensional cases, the solvability condition of the stability equations at order $O(\varepsilon)$ yields the amplitude equation satisfied by $A(X, Y)$. Without elaborating further on the exact integration of $A(X, Y)$, this amplitude equation reads in a generic form (the explicit expression can be found in chapter 3 of Martinand 2003):

$$\begin{aligned}\partial_X A\ \partial_{k_x}\omega(X, Y; \omega_0) + \partial_Y A\ \partial_{k_y}\omega(X, Y; \omega_0) + A\big\{-\mathrm{i}\omega_1 + \tfrac{1}{2}\nabla_{\boldsymbol{X}} k_x \cdot \nabla_{\boldsymbol{k}}\partial_{k_x}\omega \\ + \tfrac{1}{2}\nabla_{\boldsymbol{X}} k_y \cdot \nabla_{\boldsymbol{k}}\partial_{k_y}\omega + \nabla_{\boldsymbol{X}}\mathscr{R} \cdot \nabla_{\boldsymbol{k}}\partial_{\mathscr{R}}\omega + \Gamma_0(X, Y; \omega_0) + \Gamma_1(X, Y; \omega_0)\big\} = 0.\end{aligned} \tag{3.10}$$

In (3.10) $\nabla_{\boldsymbol{X}} = (\partial_X, \partial_Y)$, $\nabla_{\boldsymbol{k}} = (\partial_{k_x}, \partial_{k_y})$, $\Gamma_0(X, Y; \omega_0)$ gathers the contributions due to spatial derivatives of the order $O(\varepsilon^0)$, (2.4), of the basic state and $\Gamma_1(X, Y; \omega_0)$ gathers the contributions due to the order $O(\varepsilon^1)$, (2.5).

3.2. *Rays, gauge choice and WKBJ breakdown: the construction of a three-dimensional global mode*

The leading order of the WKBJ expansion is expressed in terms of the function $\Phi(X, Y)$, solution of the dispersion relation (3.8), and of the amplitude $A(X, Y)$, solution of (3.10). Both these equations are first-order partial differential equations, *a priori* with complex coefficients, and can be integrated along their characteristics. Parameterized by the curvilinear coordinate S – scaling as X and Y – the characteristics (X_c, Y_c) of both equations (3.8) and (3.10) are solutions of:

$$X_c'(S) = \partial_{k_x}\omega^S, \tag{3.11a}$$

$$Y_c'(S) = \partial_{k_y}\omega^S, \tag{3.11b}$$

the superscript S meaning that the different functions are evaluated at $(X_c(S), Y_c(S))$.[...] Along these characteristics, the variations of $\boldsymbol{k}$ and A are given by:

$$\mathrm{d}_S k_x = -\partial_{\mathscr{R}}\omega^S \partial_X \mathscr{R}^S, \tag{3.12a}$$

$$\mathrm{d}_S k_y = -\partial_{\mathscr{R}}\omega^S \partial_Y \mathscr{R}^S \tag{3.12b}$$

and

$$\mathrm{d}_S A = -A\{-\mathrm{i}\omega_1 + \Gamma(X_c(S), Y_c(S); \omega_0)\}, \tag{3.13}$$

with all of the terms due to the inhomogeneity of $\mathscr{R}$ and $\boldsymbol{k}$ as well as the terms containing contributions of order $0(\varepsilon^1)$ to the basic state in (3.10) further gathered in $\Gamma(X, Y; \omega_0)$. By casting this construction in the form of the ray-tracing method (as described in Lighthill 1978, p. 317), the optical interpretation of the WKBJ expansion is clearly evident. Integration of (3.8) and (3.10) can be performed along the characteristics given by (3.11) as long as 'gauges' for A and Φ are known on a curve intersecting all these characteristics. These integrations would also provide an upper bound for the approximation $\mathrm{Im}(\omega_0 + \varepsilon\omega_1)$ of the global mode growth rate, which would be a first step towards a selection criterion for the most unstable mode. At this point, however, the only information that can be used for the gauge choice is the boundary condition (3.9) satisfied by Φ, but it is unclear whether it always allows the necessary values A and Φ on a curve intersecting all the characteristics to be obtained with a complex frequency $\omega_0 + \varepsilon\omega_1$, which is so far arbitrary. Moreover, as equation (3.8) is nonlinear, the evaluation of the characteristics and the integration of $\Phi(X, Y)$ must be performed simultaneously. This is definitely insufficient for the integration of A and hence the leading order of the WKBJ expansion cannot, as it stands, be obtained in a straightforward manner.

Apart from the difficulty of determining the WKBJ expansion in its domain of validity, we must also investigate the possibility of its breakdown. As it is restricted to describing slowly evolving instabilities, this expansion fails to capture dramatic spatial changes such as reflections which occur at points (X^t, Y^t) where

$$\partial_{k_x}\omega^t = \partial_{k_y}\omega^t = 0, \tag{3.14}$$

i.e. where the coefficients of both first derivatives of A vanish in equation (3.10). These points, where (3.10) breaks down, are called turning points of the WKBJ approximation. The superscript t is hereinafter used to indicate that the respective quantities are to be evaluated at such a turning point. Physically, the vanishing group velocity (3.14) at a turning point is related to the reflection of an incident wave due to the local modification of the dispersion relation. From a heuristic point of view, a set of turning points delimiting a simply connected domain in physical space can

be thought of as imposing a resonance condition and associated quantizations of the wavevector and frequency via reflections in the horizontal (x, y)-plane. If this quantization implies a finite upper bound for the temporal growth rate $\mathrm{Im}(\omega_0 + \varepsilon\omega_1)$, a selection criterion for the most unstable mode results.

Following previous results for one-dimensional inhomogeneities of the RBP system (Carrière & Monkewitz 2001), we restrict this study to situations where the set of turning points coalesces into a double turning point satisfying

$$\partial_X \omega^{\mathrm{t}} = \partial_Y \omega^{\mathrm{t}} = 0. \tag{3.15}$$

In RBP convection, owing to the instability mechanism, $\mathrm{Im}(\omega(k_x, k_y, \mathscr{R}))$ is a strictly growing function of $\mathscr{R}$. Hence, generalizing results obtained within the envelope equations formalism by Carrière *et al.* (2004), the double turning point must also satisfy

$$\partial_X \mathscr{R}^{\mathrm{t}} = \partial_Y \mathscr{R}^{\mathrm{t}} = 0, \tag{3.16}$$

and is therefore located at the maximum of $\mathscr{R}(X, Y)$, i.e. at the top of the temperature bump $X^{\mathrm{t}} = Y^{\mathrm{t}} = 0$. As arbitrary as the restriction to global modes governed by a double turning point may look at this point, it will be put on firmer ground at the end of § 4.

4. Inner solution close to the double turning point and selection criterion

Since the WKBJ expansion breaks down at the double turning point, the construction of the global mode requires a separate analysis in this region. The inner solution in the vicinity of the double turning point – the WKBJ expansion becoming in retrospect the outer solution – hence requires a 'blowup' (rescaling) of the region around the top of the temperature bump.

4.1. *Leading order of the inner solution and selection criterion of the global mode*

Following exact results for double turning points in one-dimensional inhomogeneous cases (see Wasow 1985; Le Dizès *et al.* 1996, for details), the inner solution for the perturbation is sought in the form:

$$\begin{aligned}\boldsymbol{v}^{\mathrm{t}} = &\left\{\boldsymbol{v}_0^{\mathrm{t}}(\chi, \varphi, z) + \varepsilon^{1/2}\boldsymbol{v}_{1/2}^{\mathrm{t}}(\chi, \varphi, z) + \varepsilon\boldsymbol{v}_1^{\mathrm{t}}(\chi, \varphi, z) + O(\varepsilon^{3/2})\right\} \\ &\times \exp\left[\frac{\mathrm{i}}{\varepsilon^{1/2}}\left(k_x^{\mathrm{t}}\chi + k_y^{\mathrm{t}}\varphi\right) - \mathrm{i}\omega t\right] + \text{c.c.},\end{aligned} \tag{4.1}$$

where the new 'intermediate' coordinates $\chi = \varepsilon^{1/2}x = \varepsilon^{-1/2}X$ and $\varphi = \varepsilon^{1/2}y = \varepsilon^{-1/2}Y$, halfway between the 'fast' (x, y) and the 'slow' (X, Y) coordinates, have been introduced. The argument of the exponential in (4.1) comes from the leading order of $\Phi(X, Y)$ expanded around the turning point, while the frequency is still sought in the form (3.2).

Next, the basic state is rewritten in terms of the intermediate variables χ and φ and expanded about the double turning point $(x, y) = (0, 0)$.

$$U_b(\chi, \varphi, z) = \widetilde{U_0}(z) + O\left(\varepsilon^{3/2}\right), \tag{4.2a}$$

$$V_b(\chi, \varphi, z) = O\left(\varepsilon^{3/2}\right), \tag{4.2b}$$

$$\Theta_b(\chi, \varphi, z) = -\tfrac{1}{2} + \widetilde{\Theta_0}(z)\mathscr{R}_0 + \varepsilon\widetilde{\Theta_0}(z)\left[\frac{\chi^2}{2}\partial_X^2\mathscr{R}^{\mathrm{t}} + \chi\varphi\partial_X\,\partial_Y\mathscr{R}^{\mathrm{t}} + \frac{\varphi^2}{2}\partial_Y^2\mathscr{R}^{\mathrm{t}}\right] + O(\varepsilon^{3/2}). \tag{4.2c}$$

Since $\partial_X \mathscr{R}^t = \partial_Y \mathscr{R}^t = 0$, up to order $O(\varepsilon)$ only the temperature field of the basic state exhibits horizontal variations in the vicinity of the double turning point. Noting that these variations are already accounted for by the varying reduced Rayleigh number r in the envelope equation formalism (see equation (3.8) in MCM04), the results of the analysis carried out in § 3 of MCM04 for envelope formalism are then expected to be transposable to the full set of governing equations. The main steps of this analysis are summarized here.

At order $O(\varepsilon^0)$ of the inner stability equations, the homogeneous problem (3.4) pertaining to $(\chi, \varphi) = (0, 0)$ with boundary conditions (A 4) is recovered. The leading-order $\boldsymbol{v}_0^t$ of the inner solution is then sought as:

$$\boldsymbol{v}_0^t = A(\chi, \varphi)\widehat{\boldsymbol{v}_0}^t\big(k_x^t, k_y^t, \mathscr{R}_0; \omega_0; z\big). \tag{4.3}$$

Hence, the dispersion relation satisfied at the turning point

$$\omega\big(k_x^t, k_y^t, \mathscr{R}_0\big) = \omega_0 \tag{4.4}$$

together with the turning point conditions (3.14) uniquely determine the leading-order approximation ω_0 of the global mode frequency and the wavenumbers (k_x^t, k_y^t) as a function of $\mathscr{R}_0$ alone. The inhomogeneity of the system will only appear in the correction $\varepsilon\omega_1$. As obtained for one-dimensional bumps in Carrière & Monkewitz (2001), the solvability condition at order $O(\varepsilon^{1/2})$ can be satisfied without loss of generality for $\boldsymbol{v}_0^t$. Finally, the amplitude equation for the inner region obtained from the solvability condition at order $O(\varepsilon)$ reads:

$$\partial_\chi^2 A\,\frac{\partial_{k_x}^2\omega^t}{2} + \partial_\varphi^2 A\,\frac{\partial_{k_y}^2\omega^t}{2} + A\left\{\omega_1 - \partial_{\mathscr{R}}\omega^t\left(\frac{\chi^2}{2}\partial_X^2\mathscr{R}^t + \chi\varphi\,\partial_X\,\partial_Y\mathscr{R}^t + \frac{\varphi^2}{2}\partial_Y^2\mathscr{R}^t\right)\right\} = 0, \tag{4.5}$$

assuming that condition

$$\partial_{k_x}\,\partial_{k_y}\omega^t = 0 \tag{4.6}$$

is satisfied at the double turning point. As expected, (4.5) is similar to (3.10) in MCM04, obtained in envelope formalism, but, whereas condition (4.6) is a direct consequence of the dispersion relation in envelope formalism (see equation (2.7) in MCM04), the practical justification for this assumption in the present general case will have to be discussed in § 4.3.

Following the procedure in MCM04, the most unstable solution of (4.5) is found to be of the form

$$A = \exp\big(-\tfrac{1}{2}\alpha\chi^2 - \tfrac{1}{2}\beta\varphi^2 - \delta\chi\varphi\big), \tag{4.7}$$

where the coefficients α, β and δ are given by:

$$\alpha = \epsilon_1\frac{(\partial_{\mathscr{R}}\omega^t)^{1/2}\big(\partial_X^2\mathscr{R}^t\partial_{k_x}^2\omega^t + \epsilon_2\lambda\big)}{\partial_{k_x}^2\omega^t\big(\partial_X^2\mathscr{R}^t\partial_{k_x}^2\omega^t + \partial_Y^2\mathscr{R}^t\partial_{k_y}^2\omega^t + 2\epsilon_2\lambda\big)^{1/2}}, \tag{4.8a}$$

$$\beta = \epsilon_1\frac{(\partial_{\mathscr{R}}\omega^t)^{1/2}\big(\partial_Y^2\mathscr{R}^t\partial_{k_y}^2\omega^t + \epsilon_2\lambda\big)}{\partial_{k_y}^2\omega^t\big(\partial_X^2\mathscr{R}^t\partial_{k_x}^2\omega^t + \partial_Y^2\mathscr{R}^t\partial_{k_y}^2\omega^t + 2\epsilon_2\lambda\big)^{1/2}}, \tag{4.8b}$$

$$\delta = \epsilon_1\frac{(\partial_{\mathscr{R}}\omega^t)^{1/2}\partial_X\,\partial_Y\mathscr{R}}{\big(\partial_X^2\mathscr{R}^t\partial_{k_x}^2\omega^t + \partial_Y^2\mathscr{R}^t\partial_{k_y}^2\omega^t + 2\epsilon_2\lambda\big)^{1/2}}, \tag{4.8c}$$

with

$$\lambda = \left[\partial_{k_x}^2\omega^{\mathrm{t}}\partial_{k_y}^2\omega^{\mathrm{t}}\left(\partial_X^2\mathscr{R}^{\mathrm{t}}\partial_Y^2\mathscr{R}^{\mathrm{t}} - (\partial_X\,\partial_Y\mathscr{R}^{\mathrm{t}})^2\right)\right]^{1/2}, \tag{4.9}$$

and (ϵ_1, ϵ_2) the unique pair of $+1$ and -1 which leads to a bounded amplitude $A(\chi, \varphi)$, i.e. which permits us to satisfy the conditions

$$\mathrm{Re}\,(\alpha) > 0, \tag{4.10a}$$

$$\mathrm{Re}\,(\beta) > 0, \tag{4.10b}$$

$$\mathrm{Re}\,(\delta)^2 < \mathrm{Re}\,(\alpha)\,\mathrm{Re}(\beta). \tag{4.10c}$$

Solution (4.7) is obtained provided the condition

$$\mathrm{Im}\left(\partial_{k_x}^2\omega^{\mathrm{t}}\alpha + \partial_{k_y}^2\omega^{\mathrm{t}}\beta \pm \left[\left(\partial_{k_x}^2\omega^{\mathrm{t}}\alpha - \partial_{k_y}^2\omega^{\mathrm{t}}\beta\right)^2 + 4\delta^2\partial_{k_x}^2\omega^{\mathrm{t}}\partial_{k_y}^2\omega^{\mathrm{t}}\right]^{1/2}\right) < 0 \tag{4.11}$$

is satisfied. The frequency correction ω_1 compatible with the above $O(\varepsilon^1)$ solution is:

$$\omega_1 = \tfrac{1}{2}\epsilon_1\left(\partial_{\mathscr{R}}\omega^{\mathrm{t}}\right)^{1/2}\left(\partial_X^2\mathscr{R}^{\mathrm{t}}\partial_{k_x}^2\omega^{\mathrm{t}} + \partial_Y^2\mathscr{R}^{\mathrm{t}}\partial_{k_y}^2\omega^{\mathrm{t}} + 2\epsilon_2\lambda\right)^{1/2}. \tag{4.12}$$

It is noted that, strictly speaking, this result for ω_1 is obtained from the matching of the inner solution to the outer WKBJ solution, which will be briefly discussed in § 4.2. This matching has been anticipated here by requiring the amplitude to appropriately decay in all directions away from the origin. It is further remarked that this frequency correction, which contains all the effects of inhomogeneity, vanishes only in very special situations that we do not elaborate further. Furthermore, reconsider condition (4.11) which implies that $\mathrm{Im}(\omega_1) < 0$, meaning, roughly speaking, that the inhomogeneity of $\mathscr{R}$, i.e. the decrease of $\mathscr{R}$ away from the maximum $\mathscr{R}_0$ at the origin has a damping effect relative to the local absolute growth rate ω_0 at the origin, in accord with physical intuition. With these results in hand, it is finally possible to determine the most unstable global mode and the corresponding critical physical and geometrical parameters.

4.2. *Matching of the inner and outer solutions*

Expanding the spatially varying k_x and k_y in the outer region about the double turning point yields:

$$k_x = k_x^{\mathrm{t}} + \partial_X k_x{}^{\mathrm{t}} X + \partial_Y k_x{}^{\mathrm{t}} Y, \tag{4.13a}$$

$$k_y = k_y^{\mathrm{t}} + \partial_X k_y{}^{\mathrm{t}} X + \partial_Y k_y{}^{\mathrm{t}} Y. \tag{4.13b}$$

Because of assumption (4.6), the matching of the outer and inner expansions of the global mode requires:

$$\partial_X k_x{}^{\mathrm{t}} = \mathrm{i}\alpha, \tag{4.14a}$$

$$\partial_Y k_y{}^{\mathrm{t}} = \mathrm{i}\beta, \tag{4.14b}$$

$$\partial_Y k_x{}^{\mathrm{t}} = \partial_X k_y{}^{\mathrm{t}} = \mathrm{i}\delta. \tag{4.14c}$$

Returning to the discussion of § 3, the system (3.11) defining the characteristics, along which the governing equations for the leading-order WKBJ approximation must be integrated, may be simplified close to the inner region as follows:

$$X_c' = \mathrm{i}\partial_{k_x}^2\omega^{\mathrm{t}}(\alpha X_c + \delta Y_c), \tag{4.15a}$$

$$Y_c' = \mathrm{i}\partial_{k_y}^2\omega^{\mathrm{t}}(\delta X_c + \beta Y_c). \tag{4.15b}$$

The eigenvalues of system (4.15) are

$$r_\pm = \tfrac{1}{2}\mathrm{i}\left\{\partial_{k_x}^2\omega^{\mathrm{t}}\alpha + \partial_{k_y}^2\omega^{\mathrm{t}}\beta \pm \left[\left(\partial_{k_x}^2\omega^{\mathrm{t}}\alpha - \partial_{k_y}^2\omega^{\mathrm{t}}\beta\right)^2 + 4\delta^2\partial_{k_x}^2\omega^{\mathrm{t}}\partial_{k_y}^2\omega^{\mathrm{t}}\right]^{1/2}\right\} \tag{4.16}$$

and the condition (4.11) implies that $\exp(r_{\pm}S) \to 0$ as $S \to -\infty$. The double turning point is thus a stagnation point for a set of characteristics. The existence of characteristics not originating from the double turning point remains an open question, even though this situation seems physically questionable because such a characteristic would, by the propagation of A and Φ along this curve, connect two points which are infinitely distant from the unstable region.

The inner expression of the amplitude (4.7) provides the gauge for equation (3.10) by imposing the value of the amplitude on a closed (complex) curve surrounding the double turning point. Such a curve, for instance $|x|^2 + |y|^2 = c^2$ with $(x, y) \in \mathbb{C}^2$ and c arbitrarily small, can be chosen so as to intersect, as discussed in § 3, all the characteristics originating from the double turning point. System (4.14) similarly provides the gauge on this curve to evaluate the characteristics given by (3.11) and solve (3.8) along these characteristics. The behaviour of the WKBJ expansion along a characteristic is thus slaved to the inner solution and the associated selection criterion imposed by the double turning point. Therefore, as long as the global mode in $\mathbb{R}^2$ can be deduced from the integration in $\mathbb{C}^2$ along the characteristics originating from the double turning point, the instability is of an intrinsic nature. This construction of the WKBJ expansion of the global mode along characteristics would avoid the difficulties highlighted in § 5 of MCM04 which are linked to the branch-cutting of the complex wavevector components when solving the dispersion relation (3.6) for a direct integration of the amplitude equation (3.10) in $\mathbb{R}^2$.

As discussed in § 3 of MCM04, the analytical evaluation of the most unstable global mode relies practically on the physical consistency of the result. In other words, it is necessary to check case by case that one and only one set of (ϵ_1, ϵ_2) matches conditions (4.10) and that conditions (4.11) are satisfied with this set. This was found to be true for all the cases analysed so far, but it does, of course, not guarantee a solution in all cases. Removing this uncertainty would greatly improve the robustness of the global mode analysis, but establishing conditions (4.11) directly from the dispersion relation and condition (4.10) has not been possible so far. Remember also that the analytical solution (4.8) has only been possible under condition (4.6), which appears to be satisfied in the cases presented in § 4.3. It might be possible to circumvent this condition which does not have obvious physical meaning, but at this point it is not clear how restrictive this condition is. Finally, we must point out that the consistency of the global mode construction outlined here does not exclude other possibilities, such as global modes associated with a set of distinct simple turning points which would be extensions of the modes discussed in Le Dizès *et al.* (1996). Nevertheless, our limited numerical simulations of global modes (see § 5) have always produced a most amplified mode of the double-turning-point type.

4.3. *Examples with Gaussian temperature bumps of elliptical planform*

The inner amplitude (4.7) provides an analytical approximation of the global mode in the neighbourhood of the top of the temperature bump which is useful both because it takes into account the effects of the inhomogeneity of the basic flow and because it is valid where the global mode amplitude is largest:

$$\boldsymbol{v} \approx \exp\left(-\frac{\varepsilon\alpha x^2}{2} - \frac{\varepsilon\beta y^2}{2} - \varepsilon\delta xy\right) \exp\left(\mathrm{i}k_x^{\mathrm{t}}x + \mathrm{i}k_y^{\mathrm{t}}y - \mathrm{i}(\omega_0 + \varepsilon\omega_1)t\right)\widehat{\boldsymbol{v}}_0^{\mathrm{t}}(z) + \mathrm{c.c.} \qquad (4.17)$$

Reverting to physical unstretched coordinates x and y in (4.17), $\varepsilon\alpha$, $\varepsilon\beta$, $\varepsilon\delta$ and $\varepsilon\omega_1$ are expressed by replacing the derivatives ∂_X and ∂_Y in (4.8) and (4.12) by $\varepsilon\partial_x$ and $\varepsilon\partial_y$. As outlined in the Appendix, the frequency approximation $\omega = \omega_0 + \varepsilon\omega_1$, the

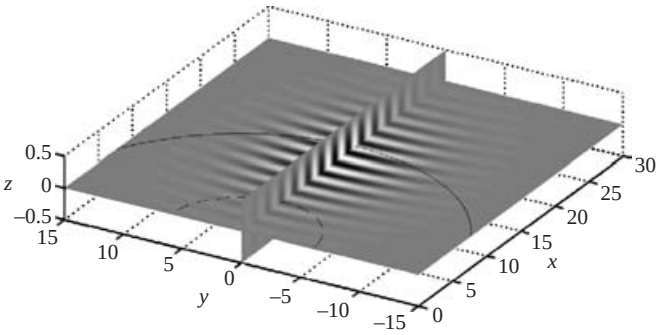

FIGURE 3. Inner turning-point approximation of the temperature field for the critical global mode with $\sigma_1 = \sigma_2 = 20$, $\mathscr{R}_0 = 1800$, $\mathscr{R}_\infty = 1500$, $P = 7$ and $R = R_{\mathrm{crit}} = 0.505$. The darker shades correspond to low temperatures and lighter shades to high temperatures of the instability. The stable/convectively unstable boundary (—) and the convective/absolute instability boundary (– – –) are superimposed on the (x, y)-plane.

wavevector at the double turning point $\boldsymbol{k}^t$ and the coefficients $\varepsilon\alpha$, $\varepsilon\beta$ and $\varepsilon\delta$ are evaluated numerically from the most unstable solution, constrained by (3.14), of the homogeneous stability problem at the top of the temperature bump.

For the generalized Gaussian bumps defined by equation (2.6) (see also figure 1), several examples of the most unstable global modes have been determined for different geometrical bump parameters σ_1, σ_2 and ψ and physical parameters $\mathscr{R}_0$, $\mathscr{R}_\infty$, R and P. An example with a round bump is shown in figure 3. Several features of this example are noteworthy. (i) The amplitude at the turning point $(x, y) = (0, 0)$ which governs the mode is small. This feature is not unexpected, as it is also characteristic of most one-dimensional global modes in open systems with through-flow as in Huerre & Monkewitz (1990). (ii) The emerging travelling rolls are seen to grow spatially in the downstream direction until they reach their maximum amplitude approximately at the most downstream point of neutral stability. This is also not surprising as it is entirely consistent with the characteristics of spatial instability waves evolving on a slowly diverging mean flow (for a jet, see e.g. Crighton & Gaster 1976). (iii) The orientation of the rolls is essentially transverse. For the circular temperature bump, this may be expected from the mirror symmetry with respect to $y = 0$, but the same transverse orientation has been observed for all the bump geometries, including skewed elliptical bumps. Expressed in more technical terms, the homogeneous stability problem at the top of the bump with the constraint (3.14) has always yielded a solution with $k_y^t = 0$, i.e. pure transverse rolls. This may be explained by the fact that in the homogeneous RBP problem only transverse rolls exhibit a transition to absolute instability (see Carrière & Monkewitz 1999), which is required at the double turning point to obtain a positive global amplification. As the inhomogeneity of the basic state does not enter the leading-order stability problem in the inner turning-point region, the rolls are expected to deviate only slightly from the transverse orientation throughout the inner region, independently of the geometrical parameters of the bump. In summary, the transverse orientation of the rolls is imposed by the mean flow direction and not by the bump geometry. This is perhaps the most surprising feature of our global mode solution, as we might think of an analogy to Rayleigh–Bénard convection in confined geometries where it has been shown by Segel (1969) and Newell & Whitehead (1969) that the wave vector aligns itself with the largest side of the convection cell. For a high-aspect-ratio elliptical temperature bump, for instance, this would suggest a

roll orientation determined by the skew angle ψ (cf. figure 1) which is clearly not compatible with our findings.

The observed selection of transverse rolls finally permits an assessment of the *ad hoc* condition (4.6). Since, owing to symmetry, k_y appears in (A 2) only as k_y^2, condition (4.6) is automatically satisfied by any solution with $k_y = 0$. Hence, condition (4.6) does not appear to be restrictive.

5. Comparison with numerical simulations

So far, the construction of the analytical global mode has relied on the assumption that the most unstable mode is associated with a double turning point at the top of the temperature bump. To assess the validity of this assumption and, by extension, of the whole analytical approach, numerical simulations of the Navier–Stokes equations subject to the Boussinesq approximation (2.1) have been performed and compared to the analytical predictions obtained in § 4.

The code used is an extension of the Navier–Stokes code developed by N. Gilbert and L. Kleiser for channel flow (see Gilbert 1988), to which the integration of the energy equation and the possibility of spatially varying boundary conditions on the horizontal plates have been added. The numerical solution is obtained by a tau-collocation pseudospectral method in space, using Fourier modes in the slowly varying directions and Chebychev polynomials in the confined vertical direction. The nonlinear terms and the diffusion terms are discretized in time by an Adams–Bashforth and a Crank–Nicolson scheme, respectively, resulting in second-order accuracy in time. As the simulation focuses on the linear and weakly nonlinear evolution of the instability, the de-aliasing of the nonlinear term in the spatial expansion of the solution is not of crucial importance and has been eliminated to decrease the computational cost. Owing to the Boussinesq approximation, the influence matrix method introduced in Kleiser & Schumann (1980, 1984) can be used to evaluate the pressure, and the pressure gradient is then discretized by an implicit Euler scheme. A characteristic of the influence matrix method is that a divergence-free flow field is forced to remain so throughout the time-integration. Hence, the initial velocity field is required to be exactly divergence-free to avoid lengthy non-physical transients. The buoyancy term, finally, is also discretized in time by an implicit Euler scheme since the energy equation (2.1*c*) is solved before the Navier–Stokes equations (2.1*b*).

A simulation is started by imposing the mean longitudinal pressure gradient in the form of a constant forcing term $-8RP$ in the momentum equation and introducing the spatially varying Rayleigh number $\mathscr{R}$ in the temperature boundary condition on the lower wall. This allows us to use the original solver for Helmholtz equations with constant coefficients written by Gilbert and Kleiser. The spectral method requires periodic conditions in both the x- and y-directions. For an arbitrary temperature bump on the lower plate, this requirement is satisfied by multiplying the spatially varying part $\mathscr{R} - \mathscr{R}_\infty$ of the boundary condition $\mathscr{R}$ by a polynomial 'hat' function which vanishes at the edges of the numerical domain. To prevent a significant modification of the spatial dependence of $\mathscr{R}$, the temperature bump has to be well inside the numerical domain. Furthermore, the periodic boundary conditions in the x- and y-directions also require the instability to vanish on the lateral boundaries in order to prevent any upstream 'contamination' by a perturbation advected beyond the downstream boundary of the numerical domain. Thus, the numerical domain has to encompass both the temperature bump and the instability. For large R, $\mathscr{R}$

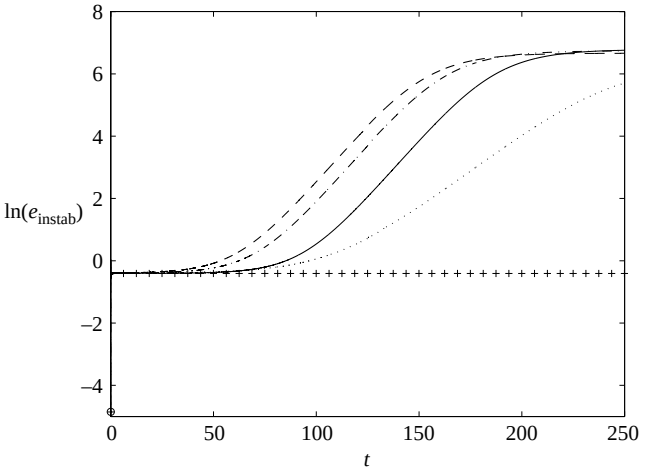

FIGURE 4. Total kinetic energy of the perturbation obtained by numerical simulations, with $R = 0.40$, $P = 7$, $\mathscr{R}_0 = 1800$, $\mathscr{R}_\infty = 1500$, $\sigma_1 = 5$, $\sigma_2 = 10$ and $\psi = \pi/4$, for grids of $32 \times 32 \times 32$ $(+\,+\,+)$, $64 \times 64 \times 32$ $(\cdots)$, $80 \times 80 \times 32$ $(-\cdot-)$, $96 \times 96 \times 32$ (—) and $108 \times 108 \times 32$ $(---)$. The circle at $t = 0$ denotes the energy level of the initial perturbation, taken to be the approximation (4.17) of the global mode.

and/or $\sigma_{1,2}$, this leads to very large numerical domains and restricts the range of the numerical simulations.

Once the computation is set up, the total field is calculated and the perturbation is determined *a posteriori* by subtracting the analytical approximation of the basic steady state (2.4) and (2.5) from the total field. This implies that the residual terms of order $O(\varepsilon^2)$ in the analytical approximation of the basic steady state are not segregated from the time-dependent perturbation and contribute to the perturbation energy.

Owing to the computational cost, convergence tests for the spatial resolution have been limited to a maximum of 108^2 Fourier modes and 32 Chebychev polynomials and are shown in figure 4. The simulations for this figure have been initialized by the sum of the steady basic flow approximation up to the order $O(\varepsilon)$, derived in § 2, and the analytical approximation (4.17) of the global mode. First, the initial jump of the perturbation energy seen in figure 4 (from the initial level $\circ$ to the level $+\,+\,+$) requires a comment: it is due to the way the perturbation is extracted from the total field for $t > 0$, i.e. to the numerically unavoidable contamination of the perturbation by the order $O(\varepsilon^2)$ correction to the basic-state initial condition, as already mentioned. In addition, the use of two consecutive identical flow fields to initialize the time integration is known to cause an additional non-physical transient with the scheme used here. Turning to the real purpose of figure 4, namely spatial resolution tests, we can see that the simulations with the $80 \times 80 \times 32$, $96 \times 96 \times 32$ and $108 \times 108 \times 32$ grids all produce time-shifted identical growth histories (identical growth rates in the linear stage and identical saturation levels), whereas the problem is clearly under-resolved by the two coarsest grids. The observed time shifts between the growth histories for the three finest grids are of no concern here, as they simply correspond to differences in the effective initial perturbation amplitude. Based on these tests, all further simulations have been performed with 96 Fourier modes in each horizontal direction and 32 Chebychev polynomials ($96 \times 96 \times 32$ basis functions)

in the numerical domain $(x, y, z) \in [-25, 25; -25, 25; -1/2, 1/2]$. For all simulations, a time step of $\Delta t = 1.25 \times 10^{-2}$ satisfied the Courant–Friedrich–Levy (CFL) condition $(\max(\|u\|) \times \Delta t)/\min(\Delta z_{\text{collocation}}) < 0.7$. At this point, it is worth going into more detail on the implementation of initial conditions.

5.1. *Initial conditions*

The initial flow field is taken to be the stationary basic flow plus a perturbation. The basic flow is approximated by (2.4) and (2.5) and the incompressibility of the velocity field is satisfied by including in the initial condition the order $O(\varepsilon^2)$ of the vertical velocity W. To avoid a bias in the selection of the most amplified global mode by the system, the initial perturbation must consist of divergence-free noise, satisfying the homogeneous boundary conditions on the horizontal plates for velocity and temperature. This is achieved by taking for the perturbation velocity the curl of a white noise and imposing $\boldsymbol{v}(z = \pm 1/2) = \mathbf{0}$ and $\theta(z = \pm 1/2) = 0$. This initial condition has been implemented in a simulation and produces the history of perturbation energy shown as a dashed line in figure 5. For this initial condition, the slow initial transient, typical of many thermal convection systems, does not completely obscure the linear stage of the instability growth, but in many other examples, the transient led directly to the nonlinear stage and it was not possible to evaluate a linear growth rate. In order to reduce the initial transient, the initial perturbation can instead be taken as the analytical global mode approximation (4.17), thereby assuming that this approximation is a good representation of the most dangerous global mode. This approach has already been used successfully in MCM04 for the integration of an envelope equation for RBP convection. The resulting evolution of the perturbation energy in the present computation is shown as the solid line in figure 5. The main result of the comparison between the two initial conditions in figure 5, is that both initial conditions produce the same global mode (compare the two snapshots at $t = 625$). Since we have not found any exception to this result, the most dangerous global mode does indeed appear to correspond to the one we have constructed around a double turning point of the WKBJ approximation.

5.2. *Comparisons between DNS and analysis*

The critical conditions, as the first result of any stability analysis, are a natural point of comparison between the analytical and the numerical results. For practical reasons, the Reynolds number is chosen here as the critical parameter, with instability for $R < R_{\text{crit}}$, while $\mathscr{R}(x, y)$ and P are kept fixed. Analytically, the selection criterion presented in § 4 yields the frequency of the global mode as a function of R, P, $\mathscr{R}_0$, $\mathscr{R}_\infty$ and of the geometrical features σ_1, σ_2 and ψ. The critical Reynolds number for the analytical global mode $R_{\text{crit}}^{\text{ana}}$ is obtained following the Appendix. For the direct numerical simulations, the critical value $R_{\text{crit}}^{\text{num}}$ is determined by interpolating the point of zero growth rate from a set of simulations for R on both sides of $R_{\text{crit}}^{\text{num}}$ (with $\mathscr{R}(x, y)$ and P fixed), as shown in figure 6. For the case considered in figure 6, the analytical and numerical critical Reynolds numbers are in excellent agreement. The difference of 0.3% is well within the expected accuracy of both the analytical approximation and the DNS. Note in the insert corresponding to $R = 0.42$, where the instability is damped, that its decay is quickly screened by the residual $O(\varepsilon^2)$ terms of the basic state. As seen in figure 7, the analytical approximation (4.17) of the global mode for the inner turning-point region captures the essential features of the global mode shape, despite the fact that the global mode is centred downstream of the turning point. Most importantly, the numerical global mode shown in figure 7(*d*) confirms the essentially transverse roll orientation predicted by the analysis. Even the slight curvature of

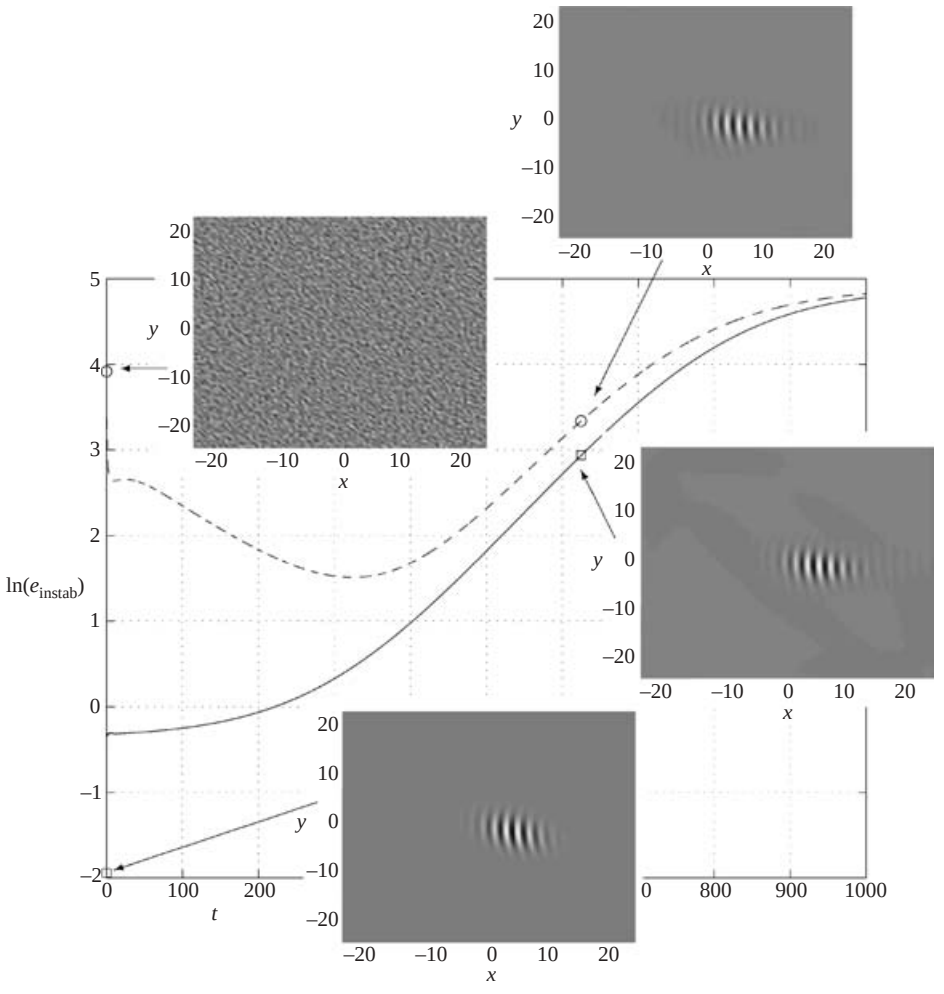

FIGURE 5. Comparison of the evolution of perturbation kinetic energy obtained with numerical simulations initialized by divergence-free noise (dashed line) and by our analytical approximation of the global mode (solid line) for $R = 0.41$, $P = 7$, $\mathscr{R}_0 = 1800$, $\mathscr{R}_\infty = 1500$, $\sigma_1 = 5$, $\sigma_2 = 10$ and $\psi = \pi/4$. For both initial conditions, snapshots of the initial perturbation at $t = 0$ and the resulting global mode at $t = 625$ near the end of the linear stage are provided in terms of the vertical component w of the perturbation velocity at $z = -0.278$. The corresponding perturbation energies are identified by $\circ$ and $\square$, respectively.

the rolls is similar in figure 7(c, d). Numerically, the maximum amplitude of the instability is found close to the downstream stability boundary, downstream of which the numerical solution exhibits a slowly damped tail which is much less pronounced for the analytical global mode in figure 7(c). It is also noted that the maximum amplitude for the analytical global mode is located slightly further upstream than for the numerical one. Both these features (shorter tail and maximum amplitude located further upstream) are due to the parabolic expansion (4.2c) of the temperature which is used to construct the inner expansion of the global mode. This expansion of the mean temperature causes $\mathscr{R}(X, Y)$ to fall off more rapidly than the Gaussian (2.6) away from the origin which explains the larger downstream damping and the small upstream shift of the analytical global mode. To improve these shortcomings of the

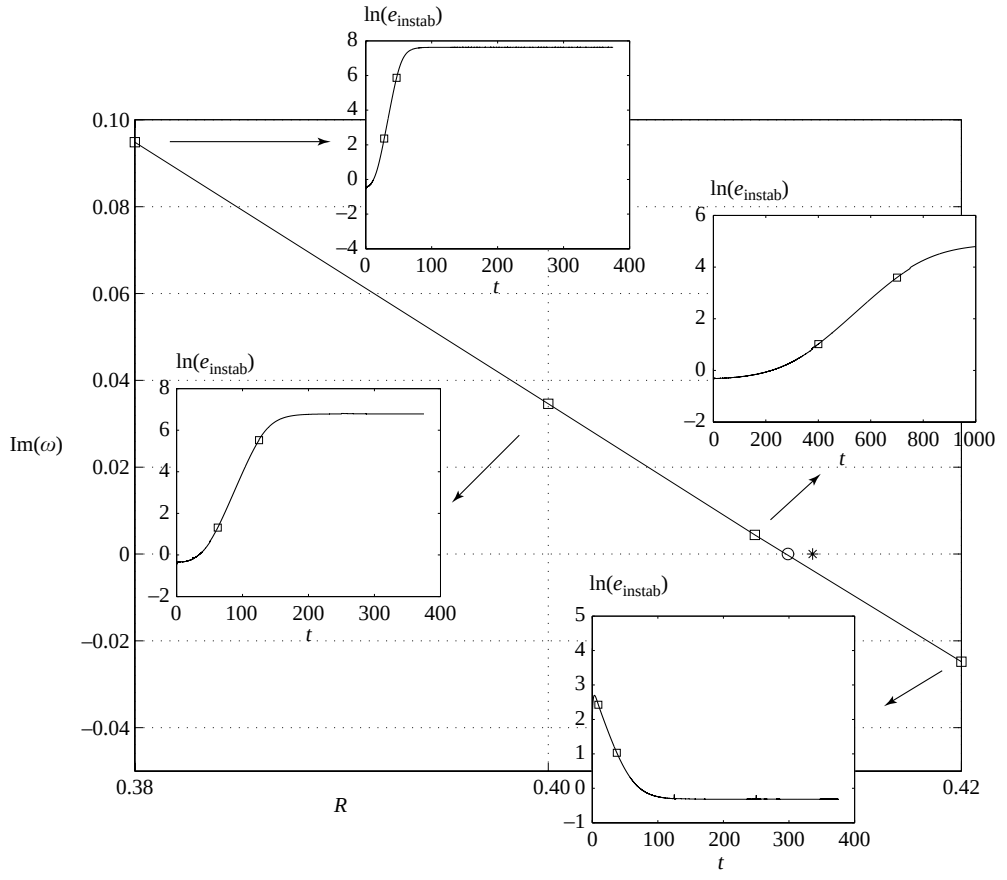

FIGURE 6. Numerical growth rates versus Reynolds number and critical Reynolds number for $\mathscr{R}_\infty = 1500$, $\mathscr{R}_0 = 1800$, $\sigma_1 = 5$, $\sigma_2 = 10$ and $\psi = \pi/4$. The growth rates (□ in the main figure) are computed from the fit to the linear part (between the □ in the four inserted figures) of the logarithm of the perturbation kinetic energy. ○ in the main figure, critical Reynolds number $R_{\text{crit}}^{\text{num}} = 0.4115$ from DNS; ∗ in the main figure, analytical $R_{\text{crit}}^{\text{ana}} = 0.4128$.

analytical approximation, the first order of the outer WKBJ expansion would have to be determined, which we did not do for the reasons outlined in § 3.

6. More discussion and outlook

As it stands, the selection criterion and the global mode approximation presented in § 4 are already useful for predicting and describing the evolution of synchronized perturbations. Furthermore, they considerably facilitate parametric studies of such instabilities owing to a reduced computational cost compared to DNS. When considering possible improvements and extensions of the analysis, the missing integration of the first-order outer WKBJ expansion, already discussed at several instances (see in particular § 3), comes to mind. Remember that this integration involves the determination of characteristics in $\mathbb{C}^2$ along which the homogeneous stability problem has to be solved. This means that the linear stability problem has to be solved for complex $\mathscr{R}$ which is uncharted territory and could dramatically restrict the feasibility of the ray tracing method. In addition it is unclear whether the physical

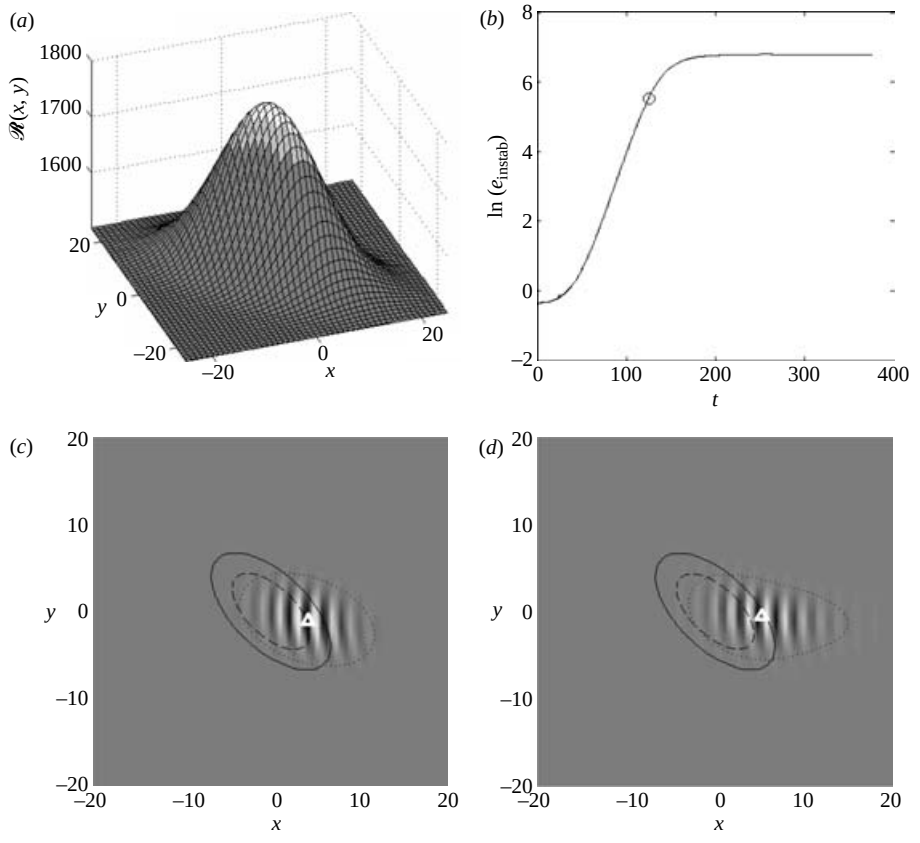

FIGURE 7. Comparison of global mode shape between analytical approximation and DNS, with $R = 0.40$, $P = 7$, $\mathscr{R}_0 = 1800$, $\mathscr{R}_\infty = 1500$, $\sigma_1 = 5$, $\sigma_2 = 10$ and $\psi = \pi/4$. (*a*) Spatial variation of $\mathscr{R}$ with superimposed local stability properties using the conventions of figure 1. (*b*) Time evolution of the kinetic perturbation energy, initialized by the analytical approximation. Vertical component of the perturbation velocity w at $z = -0.278$, (*c*) for the analytical global mode and (*d*) for the numerical simulation at $t = 125$, marked by ○ in (*b*). Superimposed on (*c*) and (*d*) are the stability boundary (– – –), the convective/absolute instability boundary (—) and the contour where the amplitude $|w|$ reaches 5 % of its maximum (· · ·), and the location of the maximum amplitude (△).

(X, Y)-plane is densely intersected by the complex rays emanating from the double turning point, i.e. whether the solution can be established on the entire (X, Y)-plane by the complex ray-tracing method developed in § 3. In short, the integration of the first-order outer WKBJ expansion appears to be a formidable task of definite mathematical interest which may not, however, be all that useful as it concerns mainly the low-amplitude parts of the global mode. In addition, for a practical situation where the instability is started by a localized impulsive forcing or by a sudden appearance of the temperature bump, we may argue that nonlinear effects become important before the low-amplitude parts of the linear mode are fully established. Therefore, we believe that it will be more useful to extend the present study to nonlinear effects than to refine the linear WKBJ analysis. Before discussing this issue, however, we are first demonstrating the usefulness of our analysis for parametric studies.

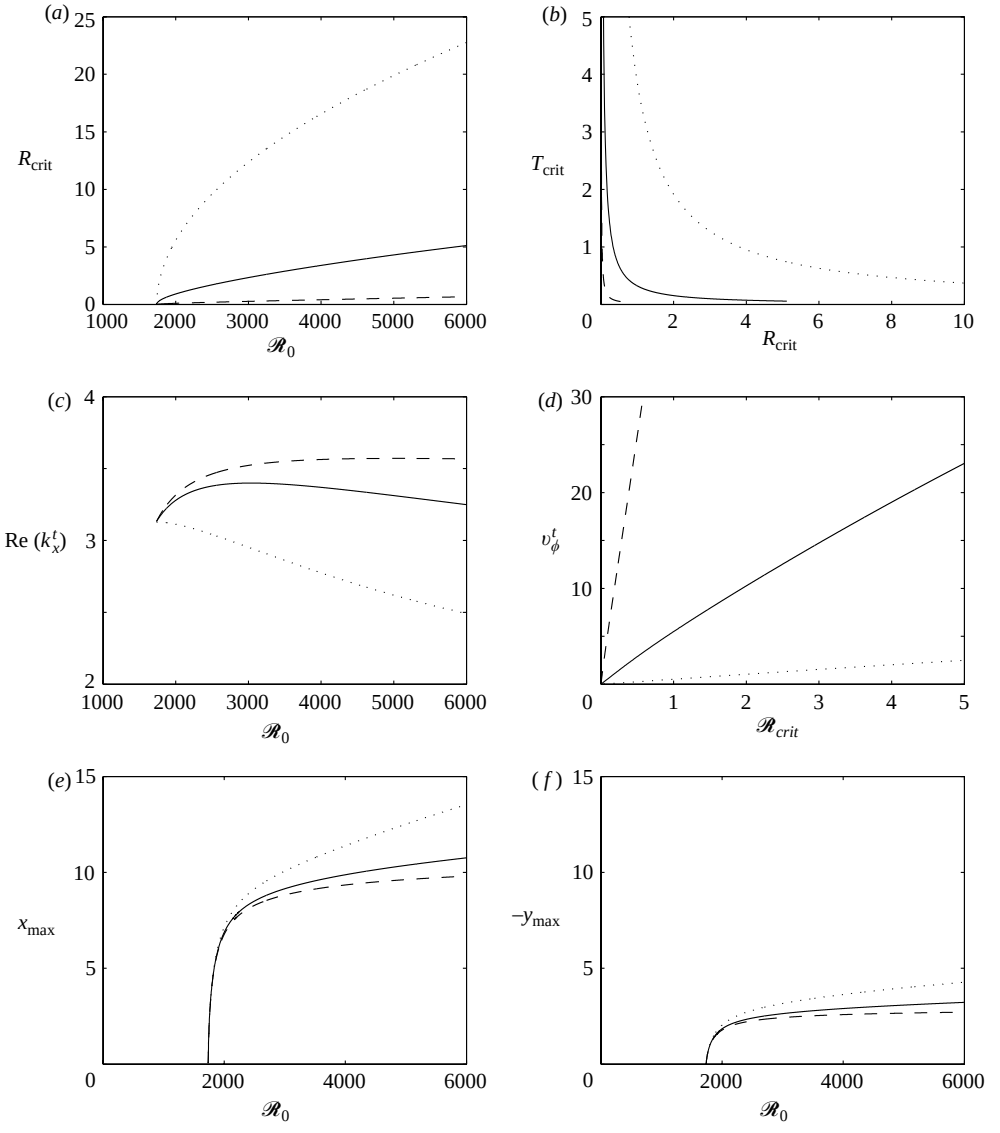

FIGURE 8. Features of the most unstable critical global mode for different Prandtl numbers $P = 0.7$ ($\cdots$), $P = 7$ (—) and $P = 70$ (— — —) with $\sigma_1 = 5$, $\sigma_2 = 10$ and $\psi = \pi/4$. (*a*) Critical Reynolds number $R_{crit}(\mathscr{R}_0)$; (*b*) temporal period $T_{crit}(R_{crit})$; (*c*) wavenumber $\mathrm{Re}(k_x^t)(\mathscr{R}_0)$, (*d*) phase velocity $(v_\phi^t)_{phys}(R_{crit})$ and location of the maximum of the instability (*e*) $x_{max}(\mathscr{R}_0)$ and (*f*) $y_{max}(\mathscr{R}_0)$.

6.1. *Parametric study*

The parametric study presented here is limited to the variation of Rayleigh number $\mathscr{R}_0$ at the top of a given temperature bump and of Prandtl number P. For more exhaustive results, see Martinand (2003). The results of this parametric study for the same skewed elliptical bump as in figures 6 and 7, are presented in figure 8 in terms of the critical Reynolds number R_{crit}, critical period $2\pi/\mathrm{Re}(\omega)$, streamwise wavenumber $\mathrm{Re}(k_x^t)$, the physically observed phase velocity $v_\phi^t = \mathrm{Re}(\omega)/\mathrm{Re}(k_x^t)$, and the location

$(x_{\max}, y_{\max})$ of the maximum amplitude of the analytical inner approximation (4.17). This maximum is obtained from the magnitude of the z-averaged inner approximation (4.17):

$$\left| \exp\left(-\frac{\varepsilon\alpha x^2}{2} - \frac{\varepsilon\beta y^2}{2} - \varepsilon\delta xy\right) \exp\left(\mathrm{i}k_x^t x + \mathrm{i}k_y^t y\right) \right|$$
$$= \exp\left(-\frac{\mathrm{Re}(\varepsilon\alpha)x^2}{2} - \frac{\mathrm{Re}(\varepsilon\beta)y^2}{2} - \mathrm{Re}(\varepsilon\delta)xy\right) \exp\left(-\mathrm{Im}\left(k_x^t\right)x - \mathrm{Im}\left(k_y^t\right)y\right). \quad (6.1)$$

From (6.1), it is immediately seen that the streamwise and lateral shifts of the point of maximum amplitude are due to non-zero spatial growth rates $(-\mathrm{Im}(k_x^t))$ and $(-\mathrm{Im}(k_y^t))$. Taking into account $k_y^t = 0$, (6.1) yields the maximum amplitude of the inner global mode approximation at

$$x_{\max} = -\frac{\mathrm{Re}(\varepsilon\beta)\mathrm{Im}\left(k_x^t\right)}{\mathrm{Re}(\varepsilon\alpha)\mathrm{Re}(\varepsilon\beta) - \mathrm{Re}(\varepsilon\delta)^2}, \quad (6.2a)$$

$$y_{\max} = \frac{\mathrm{Re}(\varepsilon\delta)\mathrm{Im}\left(k_x^t\right)}{\mathrm{Re}(\varepsilon\alpha)\mathrm{Re}(\varepsilon\beta) - \mathrm{Re}(\varepsilon\delta)^2}. \quad (6.2b)$$

It can be seen in figure 8(a) that the proportionality obtained in the homogeneous situation (see Carrière & Monkewitz 1999) $R_{\mathrm{crit}}^2 \propto (\mathscr{R} - \mathscr{R}_{\mathrm{crit}}^{RB})$, where $\mathscr{R}_{\mathrm{crit}}^{RB} = 1707.76$ is the critical Rayleigh number for Rayleigh–Bénard convection, is nearly reproduced, save for a small modification by the inhomogeneity through $\varepsilon\omega_1$ – the smallest $\mathscr{R}_{0,min}$ for which a neutral global mode can be sustained at $R = 0$, for instance, is found between 1734 and 1736, i.e. slightly larger than $\mathscr{R}_{\mathrm{crit}}^{RB}$. Furthermore, as P is decreased, the system becomes more unstable, i.e. R_{crit} increases as physically expected for decreasing viscous dissipation. This is also in accord with the trends previously observed by Carrière & Monkewitz (1999) for the convective/absolute transition in the homogeneous system. In figure 8(b), the roll passage period of the marginaly unstable mode, plotted as a function of R_{crit}, is diverging for $R \to 0$, which is consistent with the stationary cells found in the classical Rayleigh–Bénard system at marginal stability. The roll spacing, as characterized by the real part of the streamwise wavenumber shown in figure 8(c), is also seen to be relatively strongly influenced by P, with small P leading to a larger spacing as physically expected for increasing thermal diffusion. Figure 8(d), finally, reveals a nearly linear dependence of the physical phase velocity on R_{crit}.

6.2. *Preliminary study of the global mode saturation*

Numerical simulations have been used earlier in the paper to support the analytical selection criterion developed for linear global modes. Here, they are exploited to provide a preliminary picture of how these linear modes saturate. The main question addressed here is how the mode shape changes when saturation is approached. For one-dimensional slowly varying systems, Pier, Huerre & Chomaz (2001) have demonstrated the existence of two possible nonlinear evolutions: one towards a saturated 'hat'-solution characterized by a mode shape similar to the linear mode shape and pertinent to near-critical conditions, and another fully nonlinear 'elephant'-solution which develops a steep front at the upstream convective–absolute transition point. According to Pier *et al.* (2001) the latter 'steep' solution is the one realized by physical systems. A first and still incomplete survey of saturated two-dimensional global modes (modes with two wave-propagating directions) of the RBP convection tends to confirm the conclusions for one-dimensional slowly varying systems: for the

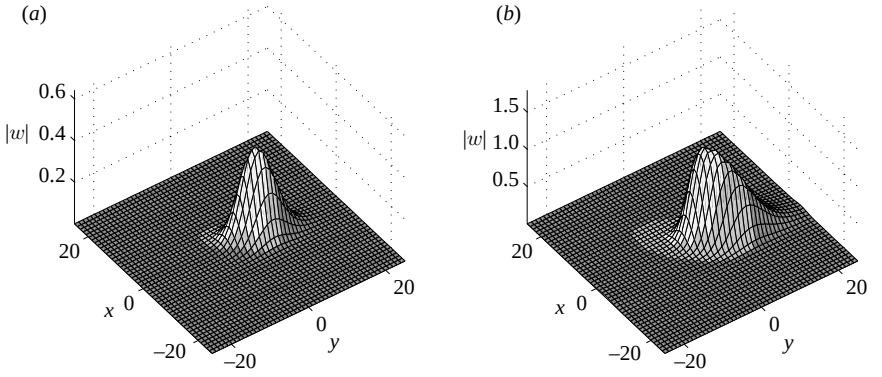

FIGURE 9. Amplitude of the nonlinear saturated state represented by the vertical component w of the perturbation velocity, for $P = 7$, $\sigma_1 = 5$, $\sigma_2 = 10$ and $\psi = \pi/4$ and (a) $R = 0.38$, $\mathscr{R}_0 = 1800$, $\mathscr{R}_\infty = 1500$, ($b$) $R = 0.85$, $\mathscr{R}_0 = 2000$, $\mathscr{R}_\infty = 1500$. The local stability prorties are superimposed using the conventions of figure 1.

example of figure 9(a) very close to critical, the global mode appears to saturate as a hat-solution, while for the conditions of figure 9(b) further from critical, the saturated mode clearly develops a steep 'nose' or three-dimensional front close to the upstream convective/absolute instability boundary. While the two examples of figure 9 look promising, a straightforward extension of the nonlinear selection criteria proposed by Pier *et al.* (2001) for one-dimensional situations to systems with two wave-propagation directions is far from obvious. For instance, already the definition of a front in two dimensions becomes fuzzy as its shape and steepness will certainly depend on the transverse curvature of the convective/absolute instability boundary. We may ask, in particular, whether the saturated mode in figure 9(a) is really a hat-solution or whether it is perhaps an elephant-solution with a nose that has been flattened by transverse curvature because of the proximity to critical conditions. Since these questions are of considerable mathematical interest and may even be of some practical interest in real, imperfect (inhomogeneous) coating devices, for instance, the thorough study of the nonlinear evolution of the global modes analysed in this paper appears to be a promising direction for future research.

We would like to thank J. F. Scott for the helpful discussions on the fine points of the WKBJ expansion as well as M. Deville and L. Kleiser for providing the basic code used for the numerical part of this work. The financial support of the ERCOFTAC Leonhard Euler Center, the Direction des Relations Internationales of the CNRS (P. C.) and the DERTT of the Région Rhône-Alpes (D. M.) are gratefully acknowledged.

Appendix. Practical evaluation of the analytical solutions

A.1. *Solution of the local stability problem*

Locally, the zeroth order of the global mode is a solution of the homogeneous linear RBP stability problem (3.4) with $\mathscr{R}$ fixed to the local $\mathscr{R}(X, Y)$. For generic eigenvector $\boldsymbol{v} = (p(z), u(z), v(z), w(z), \theta(z))^{\mathrm{T}}$ and eigenvalue ω, the problem reads

$$\mathscr{M}\boldsymbol{v} - \omega\mathscr{N}\boldsymbol{v} = \boldsymbol{0}, \tag{A 1}$$

with

$$\mathscr{M} = \begin{pmatrix} 0 & -\mathrm{i}k_x & -\mathrm{i}k_y & -\partial_z & 0 \\ \mathrm{i}k_x & \begin{matrix}+\mathrm{i}RU_0k_x \\ +k^2-\partial_z^2\end{matrix} & 0 & R\mathrm{d}_zU_0 & 0 \\ \mathrm{i}k_y & 0 & \begin{matrix}+\mathrm{i}RU_0k_x \\ +k^2-\partial_z^2\end{matrix} & 0 & 0 \\ \partial_z & 0 & 0 & \begin{matrix}+\mathrm{i}RU_0k_x \\ +k^2-\partial_z^2\end{matrix} & -1 \\ 0 & 0 & 0 & -\mathscr{R} & \begin{matrix}+\mathrm{i}RPU_0k_x \\ +k^2-\partial_z^2\end{matrix} \end{pmatrix} \tag{A 2}$$

and

$$\mathscr{N} = \begin{pmatrix} 0 & 0 & 0 & 0 & 0 \\ 0 & \mathrm{i}P^{-1} & 0 & 0 & 0 \\ 0 & 0 & \mathrm{i}P^{-1} & 0 & 0 \\ 0 & 0 & 0 & \mathrm{i}P^{-1} & 0 \\ 0 & 0 & 0 & 0 & \mathrm{i} \end{pmatrix}, \tag{A 3}$$

with $\boldsymbol{v}$ satisfying the boundary conditions:

$$u\left(z=\pm\tfrac{1}{2}\right)=v\left(z=\pm\tfrac{1}{2}\right)=w\left(z=\pm\tfrac{1}{2}\right)=\theta\left(z=\pm\tfrac{1}{2}\right)=0. \tag{A 4}$$

By taking the double curl of the linearized momentum equation and using the continuity equation, (A 1) can be recast into a system of two coupled equations involving the vertical component w of the perturbation velocity and the perturbation temperature θ:

$$\mathscr{A}\boldsymbol{u}-\omega\mathscr{B}\boldsymbol{u}=0, \tag{A 5}$$

with

$$\mathscr{A} = \begin{pmatrix} \mathrm{i}k_xR\left(U_0\left(k^2-\partial_z^2\right)+\mathrm{d}_z^2U_0\right)+\left(k^2-\partial_z^2\right)^2 & -k^2 \\ -\mathscr{R} & \mathrm{i}k_xRPU_0+\left(k^2-\partial_z^2\right) \end{pmatrix}, \tag{A 6}$$

$$\mathscr{B} = \begin{pmatrix} \mathrm{i}P^{-1}\left(k^2-\partial_z^2\right) & 0 \\ 0 & \mathrm{i} \end{pmatrix} \tag{A 7}$$

and the eigenvector $\boldsymbol{u}=(w(z),\theta(z))$ satisfying the boundary conditions:

$$w\left(\pm\tfrac{1}{2}\right)=\partial_z w\left(\pm\tfrac{1}{2}\right)=\theta\left(\pm\tfrac{1}{2}\right)=0. \tag{A 8}$$

Problem (A 5) is solved by a tau-collocation spectral method using Chebychev polynomials on 32 Gauss–Lobatto collocation points. Using the continuity equation and the definition of the vorticity, the remaining components of the velocity u and v are deduced from w and ω_z as:

$$u=\frac{1}{k^2}(\mathrm{i}k_x\partial_z w-\mathrm{i}k_y\omega_z), \tag{A 9a}$$

$$v=\frac{1}{k^2}(\mathrm{i}k_y\partial_z w-\mathrm{i}k_x\omega_z), \tag{A 9b}$$

where ω_z, the z-component of the vorticity $\boldsymbol{\omega}$, is a solution of the generalized Squire equation:

$$\partial_z\omega_z+(\mathrm{i}\omega P^{-1}-\mathrm{i}Rk_xU_0(z)-k^2)\omega_z=\mathrm{i}Rk_y\mathrm{d}_zU_0w, \tag{A 10}$$

with the boundary conditions:

$$\omega_z\left(\pm\tfrac{1}{2}\right) = 0. \tag{A 11}$$

A.2. *Determination of the double turning point*

The most unstable eigensolution of problem (A 5) for given R, P and $\mathscr{R}^{\mathrm{t}}$ is associated with a turning point if, in addition to the dispersion relation (4.4), its complex wavevector (k_x, k_y) satisfies condition (3.14). The solvability conditions of the derivatives of problem (A 5) with respect to k_x and k_y can be written as:

$$\partial_{k_x}\omega = \mathsf{A}_{k_x}[\boldsymbol{u}] - \mathsf{B}_{k_x}[\boldsymbol{u}], \tag{A 12a}$$

$$\partial_{k_y}\omega = \mathsf{A}_{k_y}[\boldsymbol{u}] - \mathsf{B}_{k_y}[\boldsymbol{u}]. \tag{A 12b}$$

System (A 12) is obtained by introducing the derivatives of operators (A 6) and (A 7) with respect to k_x and k_y: $\mathscr{A}_{k_x}$, $\mathscr{B}_{k_x}$, $\mathscr{A}_{k_y}$ and $\mathscr{B}_{k_y}$, and by using the inner product:

$$\mathsf{L}[\boldsymbol{u}'] = \int_{-1/2}^{1/2} \mathscr{L}\boldsymbol{u}' \cdot \overline{\widehat{\boldsymbol{u}}^*}\,\mathrm{d}z. \tag{A 13}$$

In (A 13), $\mathscr{L}$ is one of the operators $\mathscr{A}$, $\mathscr{B}$ and their partial deriatives with respect to k_x, k_y (and, as introduced below, $\mathscr{R}$ and R), and $\overline{\widehat{\boldsymbol{u}}^*}$ is the complex conjugate ($^-$) solution of the adjoint (*) local stability problem deduced from (A 5). The inner product (A 13) is also used to impose $[\boldsymbol{u}] = 1$ in (A 12). Numerically, the turning point is found by a two-dimensional Newton–Raphson method, iterating on $\boldsymbol{k}$ until $\partial_{k_x}\omega$ and $\partial_{k_y}\omega$ both become smaller than a threshold set at 10^{-5}. The second derivatives of ω with respect to k_x and k_y, required by the Newton–Raphson method, are obtained from the solvability conditions of the second derivatives of problem (A 5):

$$\partial^2_{k_x}\omega = 2\mathsf{A}_{k_x}[\partial_{k_x}\boldsymbol{u}] + \mathsf{A}_{k_xk_x}[\boldsymbol{u}] - 2\partial_{k_x}\omega(\mathsf{B}_{k_x}[\boldsymbol{u}] + \mathsf{B}[\partial_{k_x}\boldsymbol{u}]) - 2\omega\mathsf{B}_{k_x}[\partial_{k_x}\boldsymbol{u}] - \omega\mathsf{B}_{k_xk_x}[\boldsymbol{u}], \tag{A 14a}$$

$$\partial^2_{k_y}\omega = 2\mathsf{A}_{k_y}[\partial_{k_y}\boldsymbol{u}] + \mathsf{A}_{k_yk_y}[\boldsymbol{u}] - 2\partial_{k_y}\omega(\mathsf{B}_{k_y}[\boldsymbol{u}] + \mathsf{B}[\partial_{k_y}\boldsymbol{u}]) - 2\omega\mathsf{B}_{k_y}[\partial_{k_y}\boldsymbol{u}] - \omega\mathsf{B}_{k_yk_y}[\boldsymbol{u}] \tag{A 14b}$$

and

$$\begin{aligned}\partial_{k_x}\,\partial_{k_y}\omega \;=\; & \mathsf{A}_{k_x}[\partial_{k_y}\boldsymbol{u}] + \mathsf{A}_{k_y}[\partial_{k_x}\boldsymbol{u}] + \mathsf{A}_{k_xk_y}[\boldsymbol{u}] - \partial_{k_x}\omega(\mathsf{B}_{k_y}[\boldsymbol{u}] + \mathsf{B}[\partial_{k_y}\boldsymbol{u}]) \\ & - \partial_{k_y}\omega(\mathsf{B}_{k_x}[\boldsymbol{u}] + \mathsf{B}[\partial_{k_x}\boldsymbol{u}]) - \omega(\mathsf{B}_{k_x}[\partial_{k_y}\boldsymbol{u}] + \mathsf{B}_{k_y}[\partial_{k_x}\boldsymbol{u}]).\end{aligned} \tag{A 14c}$$

Once the double turning point is reached in $\boldsymbol{k}$-space, ω_0 is the most unstable eigenvalue, associated with the eigenvector $\boldsymbol{u}^{\mathrm{t}}$ and the different quantities (4.8) and (4.12) appearing in the analytical approximation of the global mode (4.17) are then evaluated by (A 14) expressed at this double turning point and by

$$\partial_{\mathscr{R}}\omega^{\mathrm{t}} = \mathsf{A}^{\mathrm{t}}_{\mathscr{R}}[\boldsymbol{u}^{\mathrm{t}}]. \tag{A 15}$$

Analogous to the other derivatives, it is obtained from the solvability condition of the derivative of (A 5) with respect to $\mathscr{R}$. It has been verified that, in all the cases studied, the double turning-point condition (3.16) leads to $k_y^{\mathrm{t}} = 0$, and $\partial_{k_x}\,\partial_{k_y}\omega {k_y}^{\mathrm{t}} = 0$ (see also § 4).

To compute the critical Reynolds number R_{crit}, with all other parameters fixed, the Newton–Raphson method is used to iterate on R until $\mathrm{Im}(\omega)$ becomes smaller than a threshold fixed at 10^{-4}. For this, the derivative of ω with respect to R is obtained as:

$$\partial_R \omega = \mathsf{A}_R[\boldsymbol{u}], \tag{A 16}$$

with $\mathscr{A}_R$ and the associated inner product defined as explained above.

REFERENCES

Bender, C. M. & Orszag, S. A. 1978 *Advanced Mathematical Methods for Scientists and Engineers*. McGraw–Hill.

Carrière, P. & Monkewitz, P. A. 1999 Convective versus absolute instability in mixed Rayleigh–Bénard–Poiseuille convection. *J. Fluid Mech.* **384**, 243–262.

Carrière, P. & Monkewitz, P. A. 2001 Transverse-roll global modes in a Rayleigh–Bénard–Poiseuille system with streamwise variable heating. *Eur. J. Mech.* B/*Fluids* **20**, 751–770.

Carrière, P., Monkewitz, P. A. & Martinand, D. 2004 Envelope equation for the Rayleigh–Bénard–Poiseuille system. Part 1. Spatially homogeneous case. *J. Fluid Mech.* **502**, 153–174.

Chomaz, J.-M., Huerre, P. & Redekopp, L. G. 1991 A frequency selection criterion in spatially developing flows. *Stud. Appl. Maths* **84**, 119–144.

Crighton, D. & Gaster, M. 1976 Stability of slowly diverging jet flow. *J. Fluid Mech.* **77**, 397–413.

Gilbert, N. 1988 Transition von der laminaren in die turbulente Kanalströmung. PhD thesis, DFVLR Institut für Strömungsmechanik Göttingen.

Huerre, P. & Monkewitz, P. A. 1985 Absolute and convective instabilities in free shear layers. *J. Fluid Mech.* **159**, 151–168.

Huerre, P. & Monkewitz, P. A. 1990 Local and global instabilities in spatially developing flows. *Annu. Rev. Fluid Mech.* **22**, 473–537.

Jammer, M. 1966 *The Conceptual Development of Quantum Mechanics*. McGraw–Hill.

Kelly, R. E. 1994 The onset and development of thermal convection in fully developed shear flows. *Adv. Appl. Mech.* **31**, 35–112.

Kleiser, L. & Schumann, U. 1980 Treatment of incompressibility and boundary conditions in 3-D numerical spectral simulations of plane channel flows. In *Proc. Third GAMM Conf. on Numerical Methods in Fluid Mechanics*.

Kleiser, L. & Schumann, U. 1984 Spectral simulations of the laminar–turbulent transition process in plane Poiseuille flow. In *Spectral Methods for Partial Differential Equations* (ed. R. G. Voigt, D. Gottlieb & M. Y. Hussaini), pp. 141–163. SIAM, Philadelphia.

Le Dizès, S., Huerre, P., Chomaz, J.-M. & Monkewitz, P. A. 1996 Linear global modes in spatially developing media. *Phil. Trans. R. Soc. Lond.* A **354**, 169–212.

Lighthill, J. 1978 *Waves in Fluids*. Cambridge University Press.

Martinand, D. 2003 Détermination analytique des modes globaux tridimensionnels en écoulement de convection mixte du type Rayleigh–Bénard–Poiseuille. PhD thesis, Université Claude Bernard Lyon I. http://tel.ccsd.cnrs.fr/documents/archives0/00/00/34/61/index.html.

Martinand, D., Carrière, P. & Monkewitz, P. A. 2004 Envelope equation for the Rayleigh–Bénard–Poiseuille system. Part 2. Linear global modes in the case of two-dimensional non-uniform heating. *J. Fluid Mech.* **502**, 175–197.

Monkewitz, P. A., Huerre, P. & Chomaz, J.-M. 1993 Global linear stability analysis of weakly non-parallel shear flows. *J. Fluid Mech.* **288**, 1–20.

Newell, A. C. & Whitehead, J. A. 1969 Finite bandwidth, finite amplitude convection. *J. Fluid Mech.* **38**, 279–303.

Nicolas, X. 2002 Bibliographical review on the Poiseuille–Rayleigh–Bénard flows: the mixed convection flows in horizontal rectangular ducts heated from below. *Intl J. Therm. Sci.* **41**(10).

Pier, B., Huerre, P. & Chomaz, J.-M. 2001 Bifurcation to fully nonlinear synchronized structures in slowly varying media. *Physica* D **148**, 49–96.

Provansal, M., Mathis, C. & Boyer, L. 1987 Bénard–von Kármán instability: transient and forced regimes. *J. Fluid Mech.* **182**, 1–22.

Roussopoulos, K. & Monkewitz, P. A. 1996 Nonlinear modelling of vortex shedding control in cylinder wakes. *Physica* D **97**, 264–273.

Segel, L. A. 1969 Distant side-walls cause slow amplitude modulation of cellular convection. *J. Fluid Mech.* **38**, 203–224.

Wasow, W. 1985 *Linear Turning Point Theory*. Springer.